AD-A036 045 DAVID W TAYLOR NAVAL SHIP RESEARCH AND DEVELOPMENT CE--ETC F/G 20/4
EXPERIMENTAL FORCES AND FREE-SURFACE ELEVATIONS FOR A YAWED SUR--ETC(U)
JAN 77 R B CHAPMAN

UNCLASSIFIED DTNSRDC-77-0002 NL

1 OF 1
ADA036045

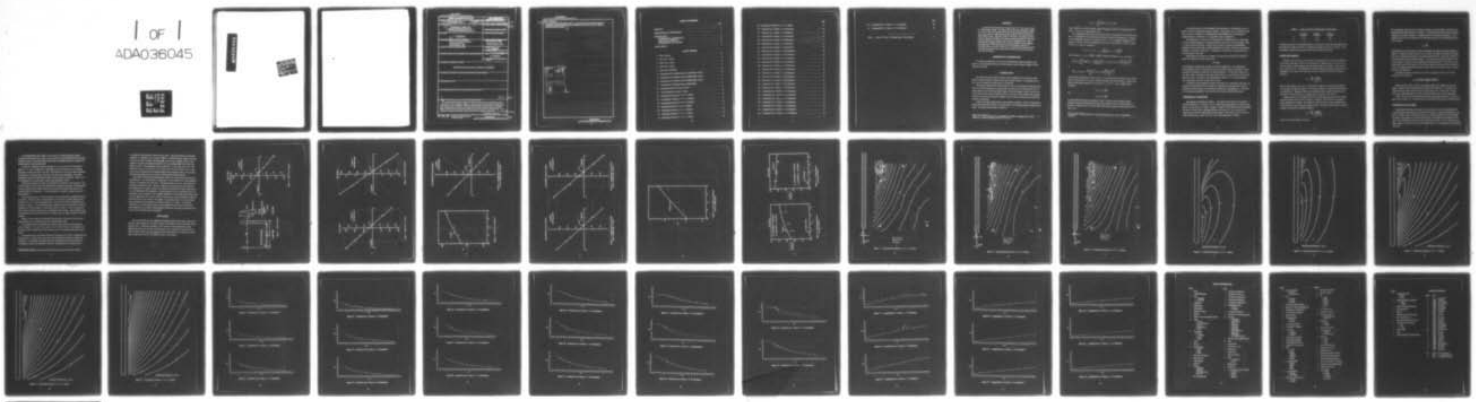

END

DATE
FILMED
3-77

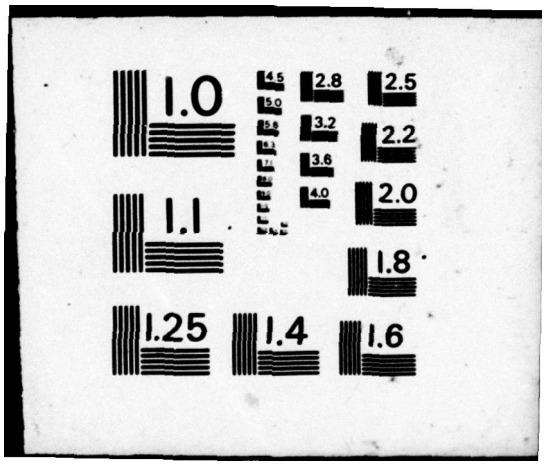
1.0
1.1
1.25
1.4
1.6
1.8
2.0
2.2
2.5
2.8
3.2
3.6
4.0
4.5
5.0

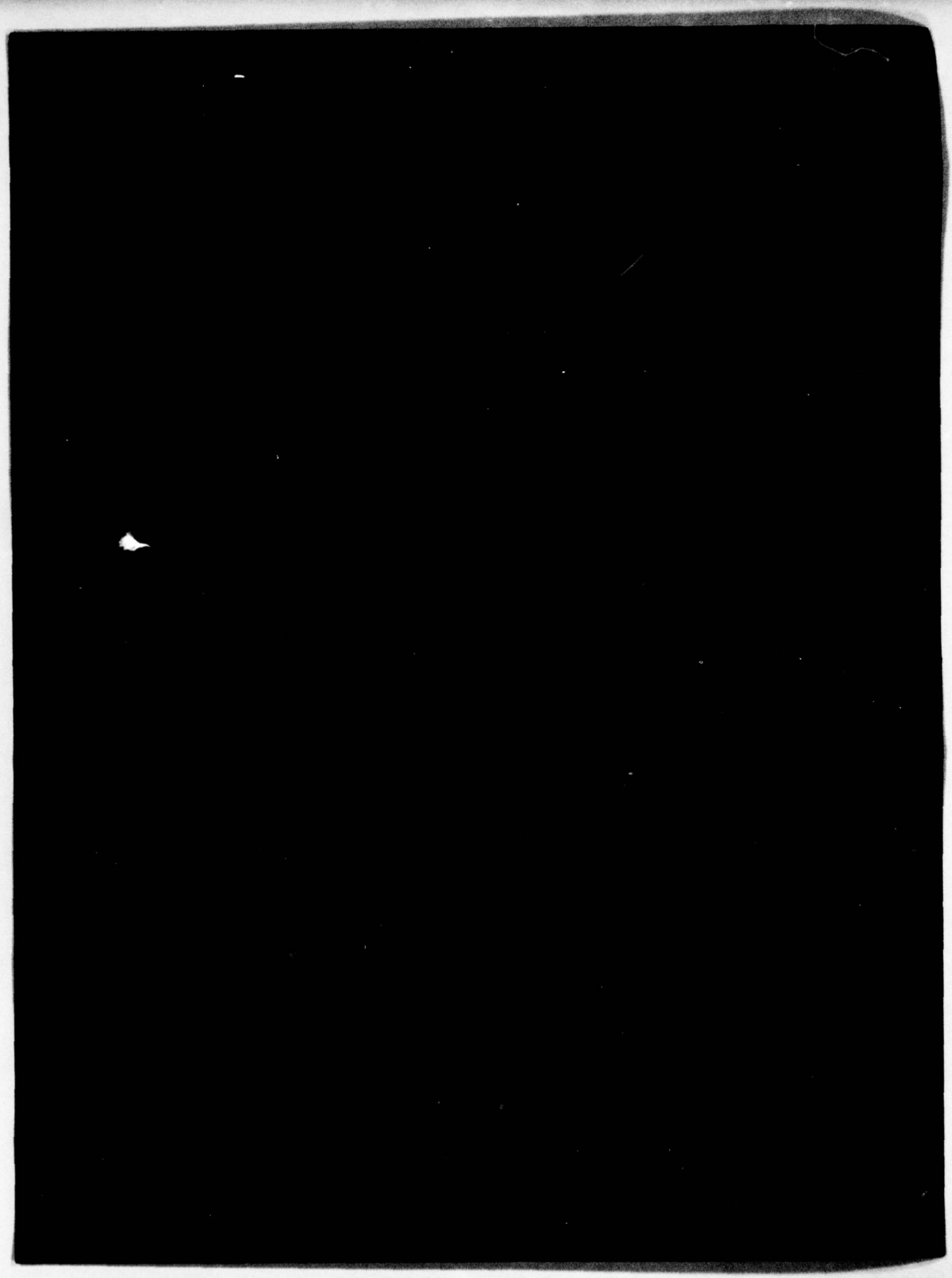

UNCLASSIFIED

SECURITY CLASSIFICATION OF THIS PAGE (When Data Entered)

REPORT DOCUMENTATION PAGE	READ DISTRUCTIONS BEFORE COMPLETING FORM
1. REPORT NUMBER (14) DTNSRDC-77/002	2. GOVT ACCESSION NO. (9) Research and development report
4. TITLE (and Subtitle) (6) EXPERIMENTAL FORCES AND FREE-SURFACE ELEVATIONS FOR A YAWED SURFACE-PIERCING PLATE	5. TYPE OF REPORT & PERIOD COVERED 6. PERFORMING ORG. REPORT NUMBER
7. AUTHOR(s) (10) R.B. Chapman	8. CONTRACT OR GRANT NUMBER(s)
9. PERFORMING ORGANIZATION NAME AND ADDRESS David W. Taylor Naval Ship Research and Development Center Bethesda, Maryland 20084	10. PROGRAM ELEMENT, PROJECT, TASK AREA & WORK UNIT NUMBERS Element Number 61153N Work Unit Number 1552-052
11. CONTROLLING OFFICE NAME AND ADDRESS	12. REPORT DATE (11) January 1977 13. NUMBER OF PAGES 38 (12) 37 pp
14. MONITORING AGENCY NAME & ADDRESS(if different from Controlling Office)	15. SECURITY CLASS. (of this report) UNCLASSIFIED 15a. DECLASSIFICATION/DOWNGRADING SCHEDULE

16. DISTRIBUTION STATEMENT (of this Report)

APPROVED FOR PUBLIC RELEASE: DISTRIBUTION UNLIMITED

17. DISTRIBUTION STATEMENT (of the abstract entered in Block 20, if different from Report)

18. SUPPLEMENTARY NOTES

19. KEY WORDS (Continue on reverse side if necessary and identify by block number)

387 682

20. ABSTRACT (Continue on reverse side if necessary and identify by block number)

A yawed surface-piercing plate of aspect ratio 0.787 was towed in water at a high Froude number. It is shown that the flow near the plate is similar to a class of flows near moving ship bows and that the free-surface elevation may be expressed as a high Froude number expansion with the initial term independent of speed. Measured values of side force, yaw moment, and roll moment indicate that slender body theory accurately predicts the forces and moments induced by an angle of attack for the conditions tested. This is confirmed by experimental free-surface contours measured by stereographic photogrammetry. → next page

(Continued on reverse side)

DD FORM 1 JAN 73 1473 EDITION OF 1 NOV 65 IS OBSOLETE S/N 0102-LF-014-6601

UNCLASSIFIED

SECURITY CLASSIFICATION OF THIS PAGE (When Data Entered)

6pg

cont

(Block 20 continued)

The experimental elevations generally conform to a theoretical prediction which superimposes the contribution of angle of attack calculated from slender body theory with the effect of thickness calculated from thin ship theory.

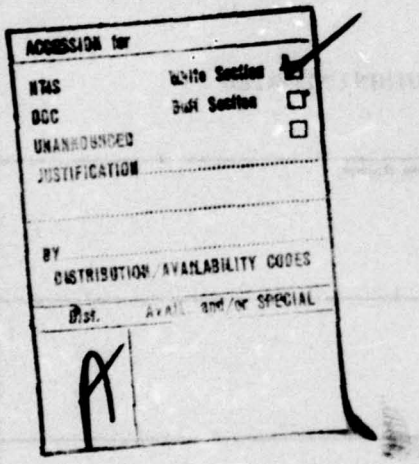

TABLE OF CONTENTS

LIST OF FIGURES

ABSTRACT

A yawed surface-piercing plate of aspect ratio 0.787 was towed in water at a high Froude number. It is shown that the flow near the plate is similar to a class of flows near moving ship bows and that the free-surface elevation may be expressed as a high Froude number expansion with the initial term independent of speed. Measured values of side force, yaw moment, and roll moment indicate that slender body theory accurately predicts the forces and moments induced by an angle of attack for the conditions tested. This is confirmed by experimental free-surface contours measured by stereographic photogrammetry. The experimental elevations generally conform to a theoretical prediction which superimposes the contribution of angle of attack calculated from slender body theory with the effect of thickness calculated from thin ship theory.

ADMINISTRATIVE INFORMATION

This work was supported by the General Hydromechanics Research Program at the David W. Taylor Naval Ship Research and Development Center, Element Number 61153N, Work Unit 1552-052.

INTRODUCTION

The free-surface characteristics of the flow near a high-speed yawed surface-piercing plate are similar to those of a class of flows near the bows of ships. A yawed plate can, in fact, serve as a model for the fine bow of a turning ship.

If the Froude number based on body draft, h, is not too small, gravity should have little effect on the flow produced by a moving surface-piercing body in a restricted area near the leading edge, even if the Froude number based on total body length is small. The flow near a ship's bow is, under certain conditions, similar to flow past a body at high Froude number. This point of view, first advocated by Ogilvie[1] may be, perhaps, illustrated by the following hueristic considerations.

A body moves with steady speed U in the negative x-direction. Let $\xi(x, y)$ represent the steady linear free-surface elevation. The x-axis starts at the leading edge and is positive downstream. The steady elevation may be written as

[1] Ogilvie, T.F., "The Wave Generated by a Fine Ship Bow," University of Michigan, Dept. of Naval Architecture and Marine Engineering, Report 127 (Oct 1972).

$$\xi(x, y) = \int_{-\infty}^{x} \xi^*(\bar{x}, y, u^{-1}(\bar{x} - x))\, d\bar{x}$$

where $V \delta t\, \xi^*(x, y, t)$ is the elevation caused by impulsive motion of the body with speed V from $t = 0$ to $t = \delta t$ as δt approaches zero.

Two assumptions will be made concerning the effect of body draft h on the free surface. First, it is assumed that the wave elevation effectively vanishes some distance $x_A < h$ ahead of the leading edge. Further, it is assumed that $\xi^*(x, y, o)$ is composed primarily of wavelengths of order 2h. The corresponding frequencies are of order $\sqrt{g/h}$. If $t^2\, gh^{-1}$ is small, then $\xi^*(x, y, t)$ may be expanded as

$$\xi^*(x, y, t) = \xi^*(x, y, o) - \left(\frac{t^2 g}{h}\right) \xi_1^*(x, y) + 0\left(\frac{t^2 g}{h}\right)^2$$

Thus, whenever $(x + x_A)\, u^{-1}\sqrt{g/h} = t\sqrt{g/h}$ is small, the elevation may be expressed as

$$\xi(x, y) = \int_{-x_A}^{x} d\bar{x}\, \xi^*(\bar{x}, y, o) - \left(\frac{g}{hu^2}\right) \int_{-x_A}^{x} (\bar{x} - x)^2\, \xi_1(\bar{x}, y)\, d\bar{x} + 0\left(\frac{g(x + x_A)^2}{hu^2}\right)^2$$

or

$$\xi(x, y) = a_0(x, y) - \frac{g(x + x_A)^2}{hu^2}\, a_1(x, y) + 0\left(\frac{g(x + x_A)^2}{hu^2}\right)^2$$

This form of an expansion in powers of $g\ell u^{-2}$ with an initial term independent of speed and gravity is characteristic of the surface elevation produced by a body moving at a high Froude number if the length parameter ℓ is replaced by $(x + x_A)^2\, h^{-1}$. If the nondimensional parameters

$$\bar{x} = x\, u^{-1} \sqrt{g/h}$$

and

$$\bar{h} = h\, u^{-1} \sqrt{g/h}$$

are both sufficiently small, the expansion is valid. Of course, practical limits on these parameters cannot be determined from this type of argument alone. Numerical results in Reference 2 suggest, however, that the high Froude number expansion remains valid for $\bar{x}$ as large as two.

---

[2] Chapman, R.B., "Free Surface Effects for Yawed Surface Piercing Plates," Journal of Ship Research (Sep 1976).

A theoretical solution for the free-surface flow generated by a moving body should, in general, require three-dimensional analytic methods. Bodies which can be considered slender are an exception. Solutions for surface-piercing slender bodies have been developed for wedge-shaped bows in Reference 1 and yawed flat plates in Reference 2.

The slenderness of a body may be characterized by its slenderness ratio ϵ representing the ratio of body dimensions, in the plane transverse to the flow, to the body length. When ϵ is small, the three-dimensional problem may be treated as a series of two-dimensional problems in the transverse plane coupled through the free surface. The flow in each plane is dependent of conditions downstream. Consequently, no disturbance is predicted ahead of the leading edge of the body.

When slender body solutions are applied to the high Froude number flows discussed above, the slenderness criterion requires that

$$\bar{h} < O(\bar{x}\epsilon)$$

This condition, combined with the limit on $\bar{x}$ restricts application to very high Froude numbers based on draft. In many practical cases, the body is thin but not slender. That is all transverse dimensions except draft are small compared to x, but the aspect ratio h/x is not small. There are indications that slender body theory for a yawed plate is valid at fairly high aspect ratios. Theoretical forces and moments in Reference 2 are in good agreement with experimental values for an aspect ratio of 0.50.

To further test the limitations of slender body theory for a yawed plate, side force, yaw moment, and roll moment were measured on a towed plate with an aspect ratio of 0.787. Contours of surface elevation were recorded and analyzed by photogrammetry. These data are in good general agreement with theoretical values based on slender body theory.

EXPERIMENTAL PARAMETERS

Plate geometry is illustrated in Figure 1. The length is 30.5 inches (77.5 cm) with a maximum thickness of 1.0 inches (2.54 cm). Bottom and leading edges are rounded to half circles. The tail section is a wedge extending 3.5 inches (8.9 cm) forward of the trailing edge. The plate was tested with a submerged depth of 24.0 inches (61.0 cm) at positive and negative angles of attack ranging from up to five degrees. Plate speeds of 4.0, 5.0, and 6.0 knots corresponding to values of $\bar{h}$ and $\bar{x}$ at the trailing edge given in TABLE 1.

TABLE 1 – Values of $\bar{h}$ and $\bar{x}$ (Trailing Edge) at Three Speeds

	4.0 Knots	5.0 Knots	6.0 Knots
$\bar{x}$	1.51	1.21	1.01
$\bar{h}$	1.19	0.95	0.79

The plate was towed in the Deep-Water Basin at the David W. Taylor Naval Shir R&D Center. This basin has a width of 51 feet (15.5 meters) and a depth of 22 feet (6.7 meters). These dimensions are large enough to assure the absence of wall or depth effects.

FORCES AND MOMENTS

Side force, yaw moment, and roll moment were measured twice at each test condition. All are linear with angle of attack over the range tested. Measured values of side force Y at the three speeds are plotted against angle of attack in Figures 2 through 4. Note that side force is zero at $\theta = 0.7$. This indicates some unintentional plate asymmetry such as twist or misalignment. The slopes of the data may be used to compute the side force coefficient defined as

$$C_Y = \frac{180}{\pi} \frac{dY/d\theta}{\frac{1}{2}\rho h^2 u^2}$$

where ρ is the density of the water. This side-force coefficient is shown plotted against $\bar{x}$ over the range investigated in Figure 5. Also shown in Figure 5 is the theoretical prediction from Reference 2. Agreement between the prediction based on slender body theory and experiment is much better than one might expect for an aspect ratio of 0.787.

Measured values of yaw moment M about the leading edge of the plate at three speeds are plotted against angle of attack in Figures 6 through 8. Note that the θ intercepts are slightly larger than 0.7 degrees. This indicates that the force due to plate asymmetry acts further aft than the force induced by angle of attack. The slopes of these data were used to compute a yaw moment coefficient defined as

$$C_M = \frac{180}{\pi} \frac{dM/d\theta}{\frac{1}{2}\rho h^2 u^2 \ell}$$

where ℓ is the chord length of the plate.

The experimental values of the yaw moment coefficient are plotted against $\bar{x}$ along with the theoretical values from Reference 2 in Figure 9. It should be noted that the above definition computes yaw moment, whereas it is computed about the midchord in Reference 2. Yaw moment data may also be expressed by the horizontal positions from the leading edge of the center of force.

$$X_f = \frac{M}{Y}$$

Experimental values of X_f/chord at positive and negative five degrees are plotted against $\bar{x}$ in Figure 10. Differences between values of X_f at positive and negative five degrees are largely due to the unintentional asymmetry in the plate mentioned above. Also shown in Figure 10 is the theoretical prediction from Reference 2. Note that the experimental positions of the center of force are forward of those predicted by slender body theory. This must be a free surface effect since in the absence of a free surface, slender body theory places the center of force at the leading edge while experiments at finite aspect ratio show the center of force to be aft of the leading edge.

Experimental values of roll moment may also be expressed in terms of the vertical position of the center force

$$Z_f = \frac{\text{roll moment (about waterline)}}{Y}$$

Measured values of Z_f/h at positive and negative angles of five degrees are plotted in Figure 11 against $\bar{x}$ along with theoretical predictions from Reference 2. Theoretical and experimental values agree within the limits of experimental error. Perhaps this is because Z_f/h is only weakly dependent on Froude number and aspect ratio over the range tested.

Overall, the side force and moment data indicate that slender body theory is valid at an aspect ratio of nearly 0.8. A more critical test is provided by measured wave height elevations.

FREE-SURFACE ELEVATIONS

Free-surface elevations near the plate were recorded with a pair of Hasselblad MK 70 cameras mounted approximately 0.9 meters above the flow on a bracket perpendicular to the plate. The field of view of the inboard camera was partially blocked by a beam connecting the plate to force gauges so that stereoscopic data are not available directly adjacent to the plate. The unobstructed stereoscopic region extended from about 2-1/2 cm outboard of the plate centerline to about 23.0 cm and from slightly ahead of the leading edge to approximately 26 cm aft.

To photograph the water surface, it was necessary to spread small paper markers (computer card punches) over a patch of water and take the photographs as the plate passed through the patch. Free-surface elevations have been successfully analyzed* at positive five degrees angle of attack (pressure side).

Contours at 3 millimeter intervals measured at 4.0, 5.0, and 6.0 knots are shown in Figures 12, 13, and 14, respectively. These figures show that elevations are not strongly dependent on speed over much of the flow. The elevations at 5 knots are shifted somewhat, due possibly to a transient wave in the tank at the time of the photograph. The speed independent term in the high Froude number expansion appears to dominate. Only in the far downstream flow near the plate is strong speed dependence evident.

Theoretical free-surface contours were calculated for comparison with experiment. The effects of angle of attack and of plate thickness were calculated separately and superimposed. The wave elevation due to angle of attack was calculated from slender body theory for a yawed flat plate as in Reference 2. To this component of elevation is added the effect of finite thickness.

The wave elevation due to the plate thickness was calculated from a simplified thin ship formulation. The nose section was represented by a line source of constant density $ut/4\pi$ located at 0.25 t aft of the leading edge, where t is the plate thickness, extending from the waterline to depth h. The wave elevation due to this line source was calculated by numerical integration of a double integral at each Froude number of interest. To this was added the effect of the tail section represented by a rectangular surface of sinks. Only the high Froude number limited was used for the tail section, however, since the region of interest is entirely upstream.

Figures 15 and 16 show the theoretical wave elevations at 4.0 and 6.0 knots for zero angle of attack; i.e., the elevations due to the thickness effect alone.

The combined effects of thickness and a positive angle of attack of five degrees are shown in Figures 17, 18, and 19 for speeds of 4.0, 5.0, and 6.0 knots. The contribution of the angle of attack vanishes ahead of the leading edge since it is derived from slender body theory.

These results may be most easily interpreted if presented in the form of longitudinal and transverse cuts. A series of such cuts at 4.0, 5.0, and 6.0 knots are shown in Figures 20 through 45. In these figures, the points where the experimental wave elevations cross the 3.0 millimeter contours are indicated by asterisks. Interpolation was used between the

*Photogrammetric analysis was performed by Photo Services Incorporated of Gaithersburg, Maryland.

3.0 millimeter intervals when contours were far apart. The lines represent the theoretical prediction. Coordinates (x, y, z) shown in Figure 1 are defined with the origin at the intersection of the plate centerline, the leading edge, and the static waterline with the x-axis parallel to the plate and positive downstream, the y-axis perpendicular to the plate and x positive upwards. The longitudinal cuts are located at y = 4 cm, 8 cm, and 12 cm. The transverse cuts are at 4 cm, 8 cm, 12 cm, 16 cm, and at 5.0 and 6.0 knots, 23 cm. The scale of these elevations has been doubled relative to the horizontal scales x and y so that the free-surface slopes are twice as steep in the plots than actually measured.

These results show good general agreement between the measured elevations and the theoretical line. It is expected that the component of wave elevation due to plate thickness would be in agreement since the theory is three-dimensional in this case, and the thin ship approximation should be valid. However, a large part of the theoretical wave elevation is the component due to angle of attack, which has been calculated from slender body theory. It can be inferred that this component is in good agreement with the experiment data for a plate aspect ratio of nearly 0.8. One possible explanation for why slender body theory holds at such a large aspect ratio is that an angle of attack induces a dipole distribution normal to the plate which, in turn, induces a flow largely in the transverse plane, so that the slender body assumption itself is satisfied even though the plate is not slender. The thickness component, on the other hand, induces a source distribution which induces velocities of equal magnitude in the transverse and longitudinal directions, satisfying thin ship approximation but not the slender body approximation.

CONCLUSIONS

Force and moment data for a high-speed yawed plate indicate that slender body theory provides a valid estimation of the effects induced by the angle of attack of an aspect ratio as large as 0.787. A theoretical prediction of wave elevation which superimposes a three-dimensional estimate of the effect of finite thickness with a slender body estimate for the effect of angle of attack is in good agreement with experimental wave elevations for a plate with an aspect ratio of 0.787 at an angle of attack of five degrees.

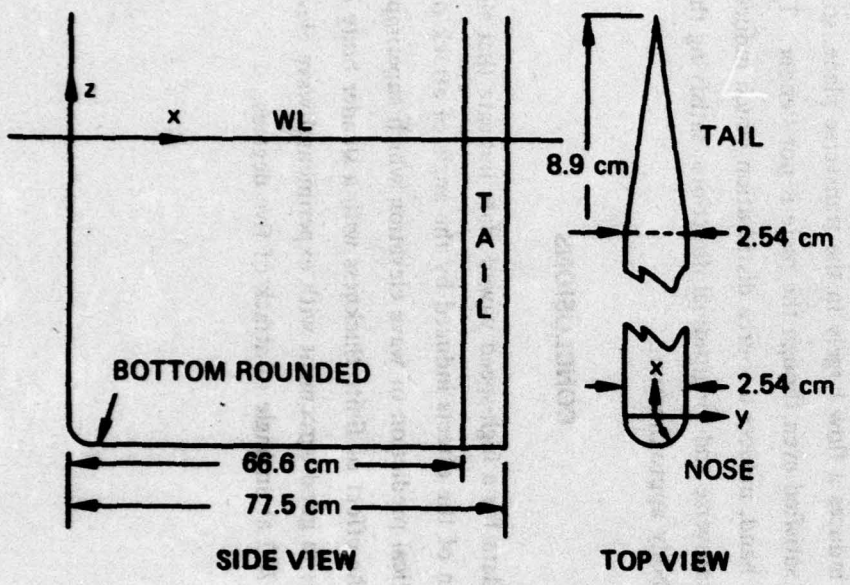

Figure 1 – Plate Geometry

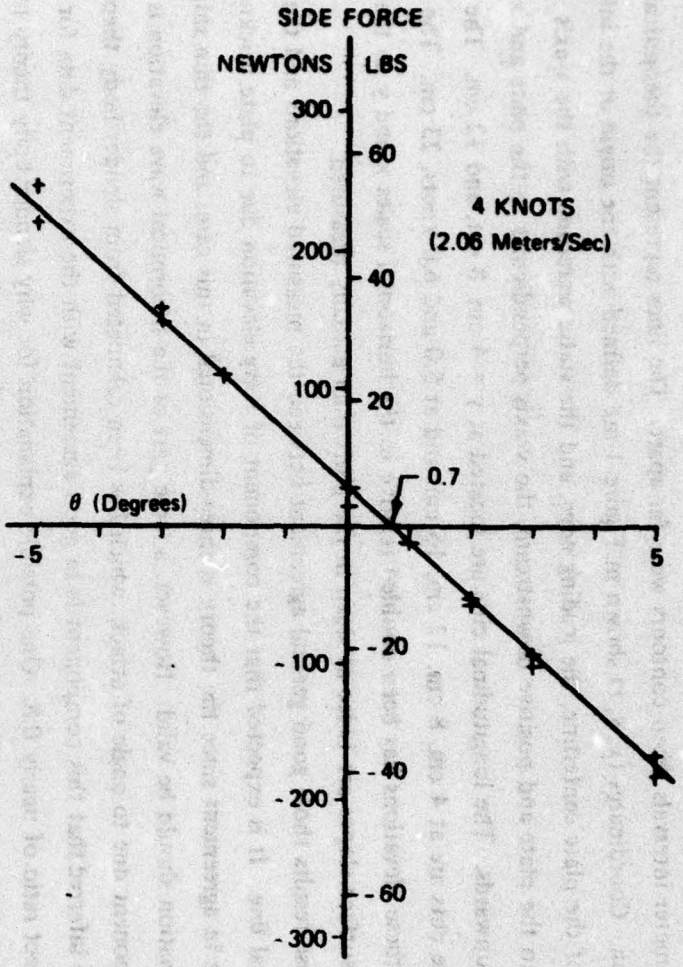

Figure 2 – Side Force, 4 Knots

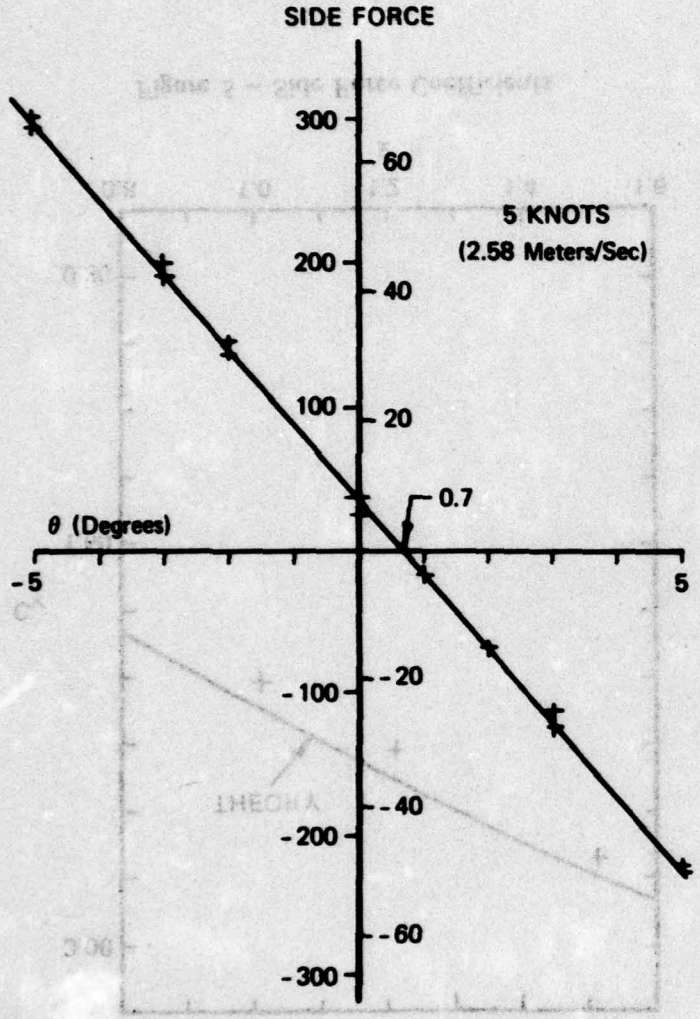

Figure 3 – Side Force, 5 Knots

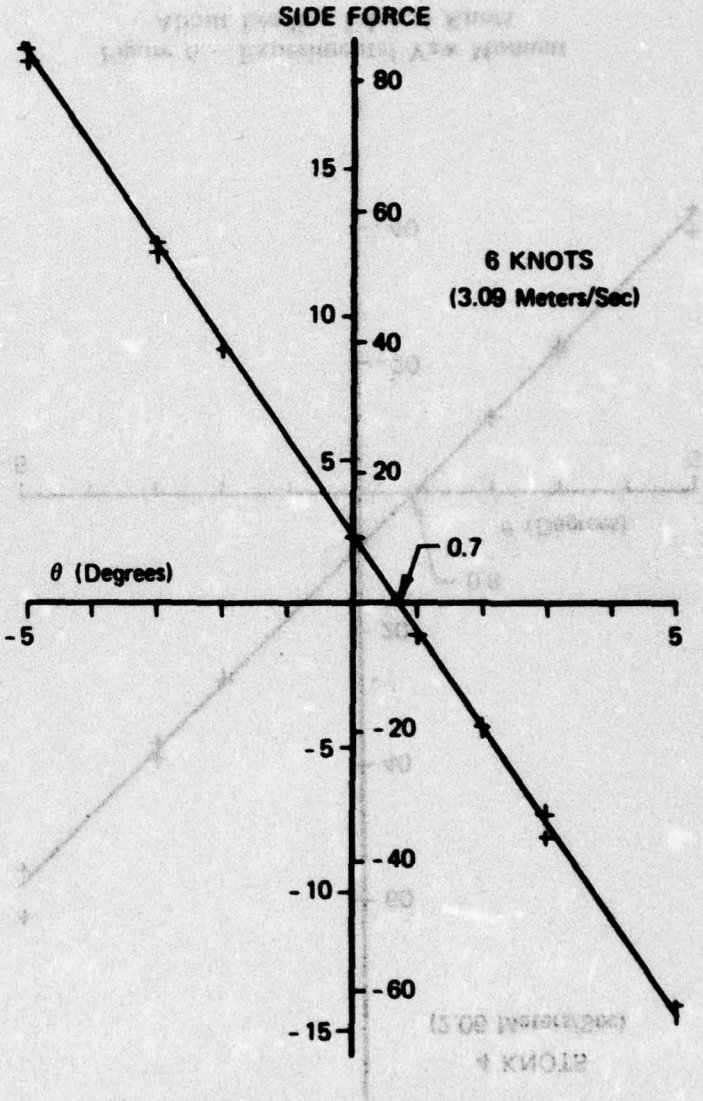

Figure 4 – Side Force, 6 Knots

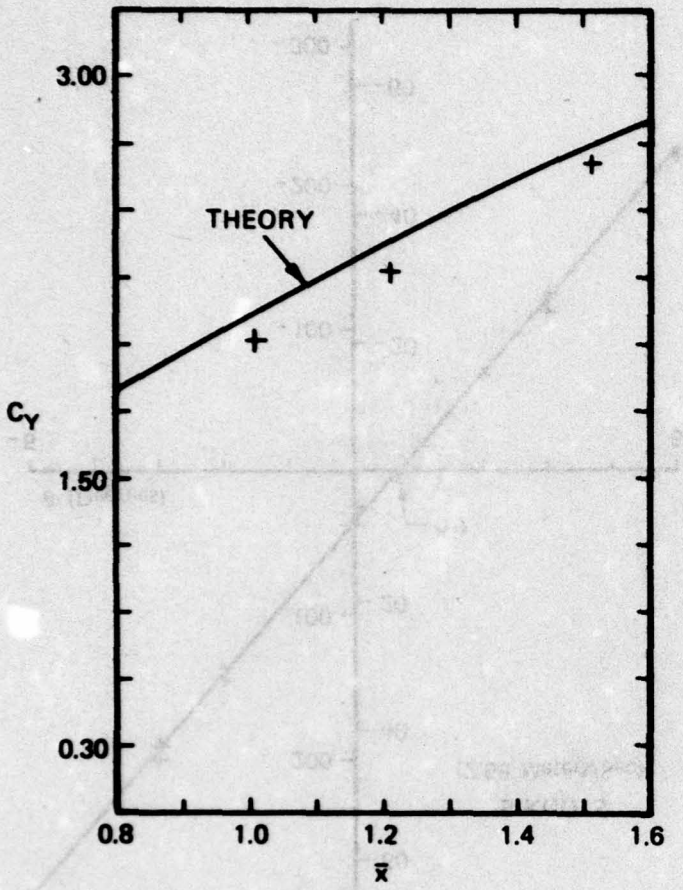

Figure 5 – Side Force Coefficients

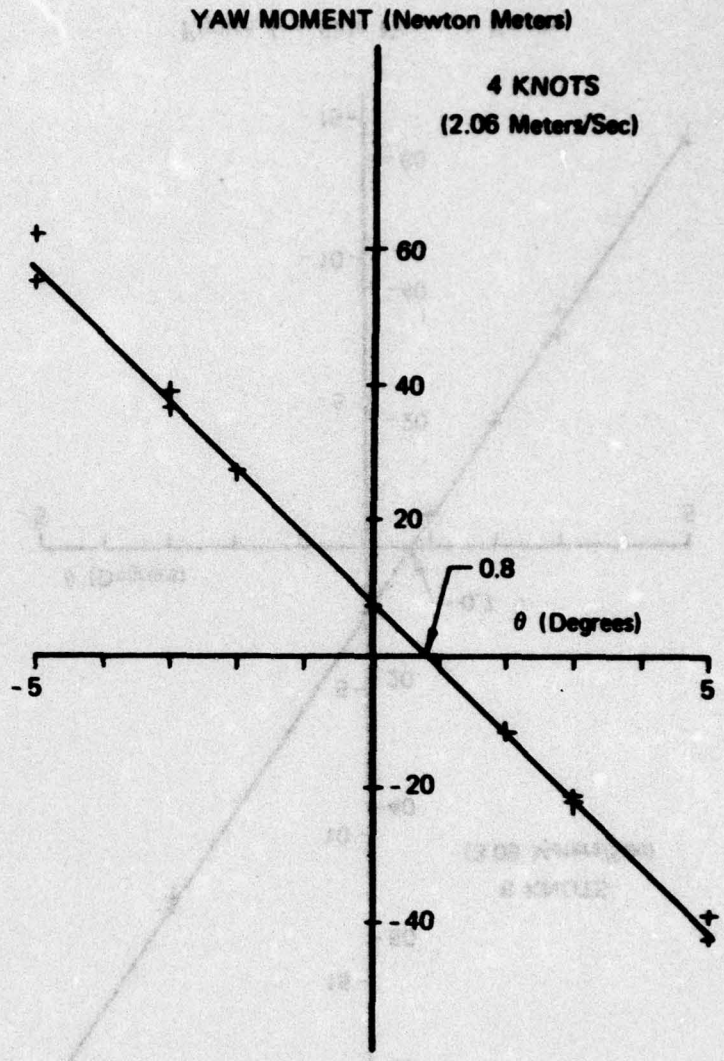

Figure 6 – Experimental Yaw Moment
About Leading Edge, 4 Knots

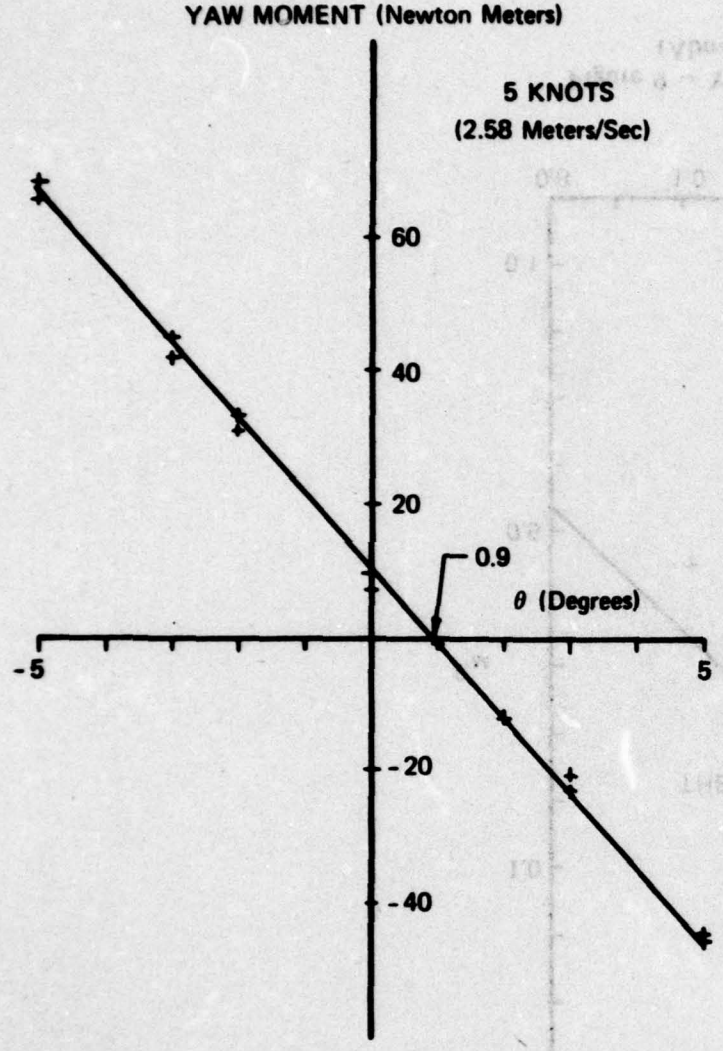

Figure 7 – Experimental Yaw Moment About Leading Edge, 5 Knots

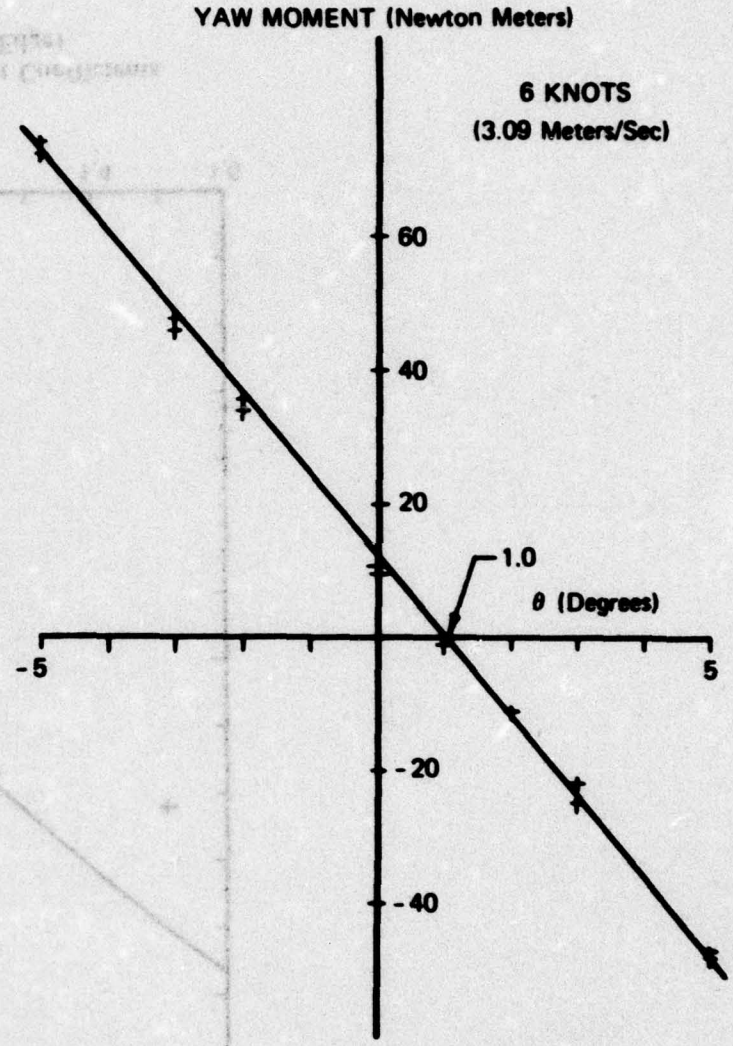

Figure 8 – Experimental Yaw Moment About Leading Edge, 6 Knots

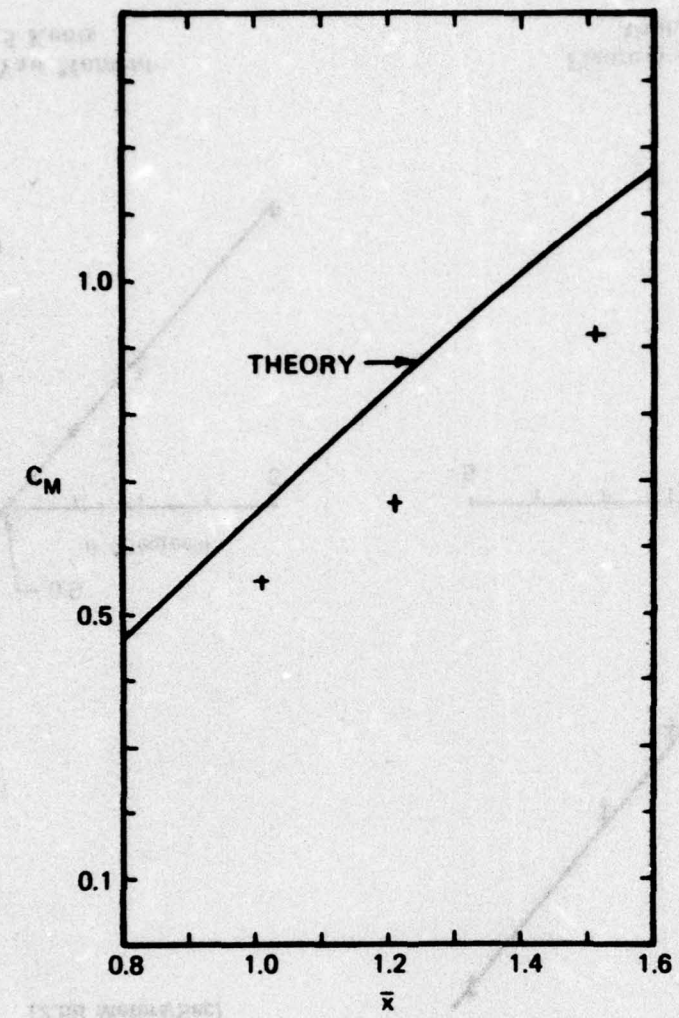

Figure 9 – Yaw Moment Coefficients (About Leading Edge)

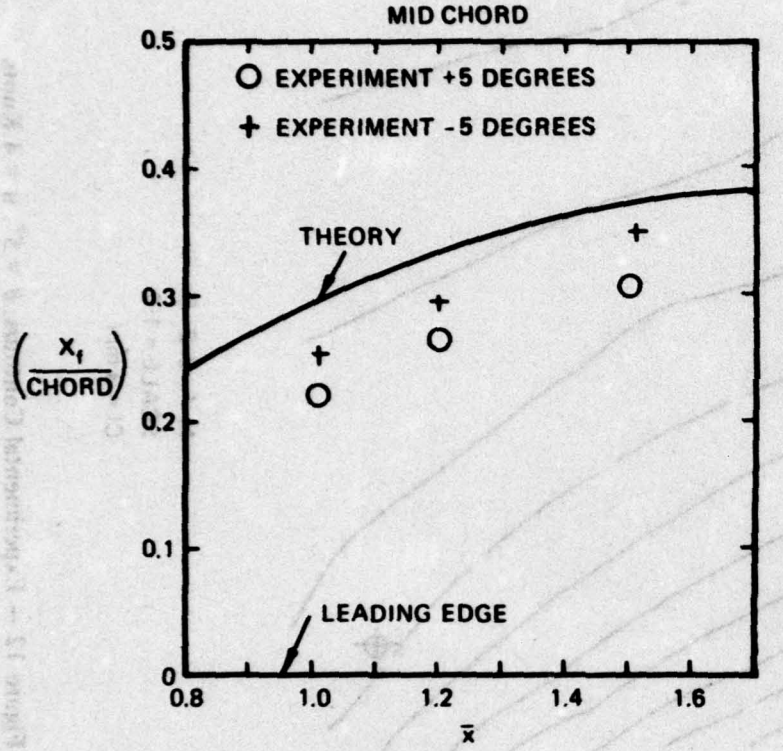

Figure 10 – Horizontal Position of Center of Force

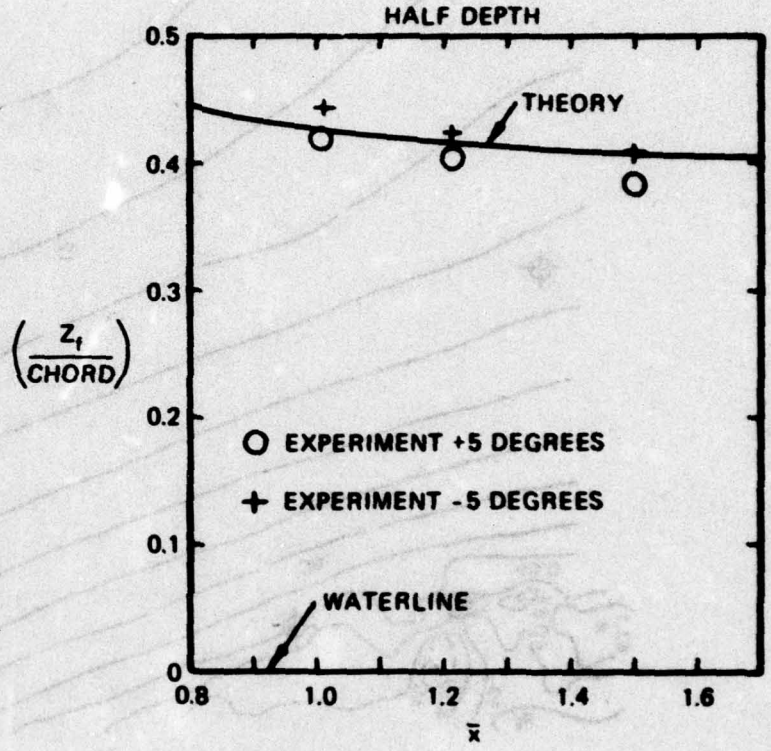

Figure 11 – Vertical Position of Center of Force

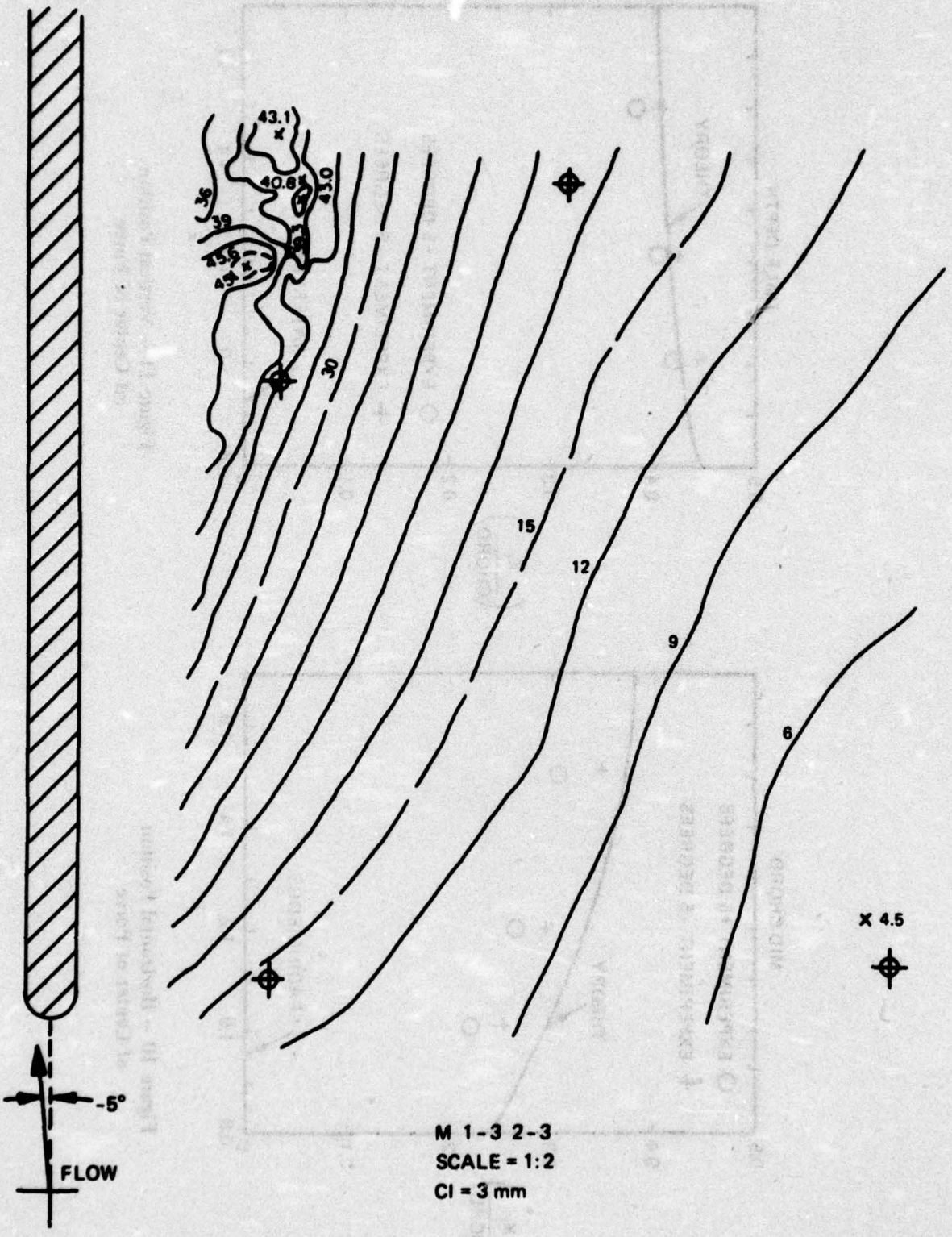

Figure 12 — Experimental Contours, $\theta = 5°$, u = 4 Knots

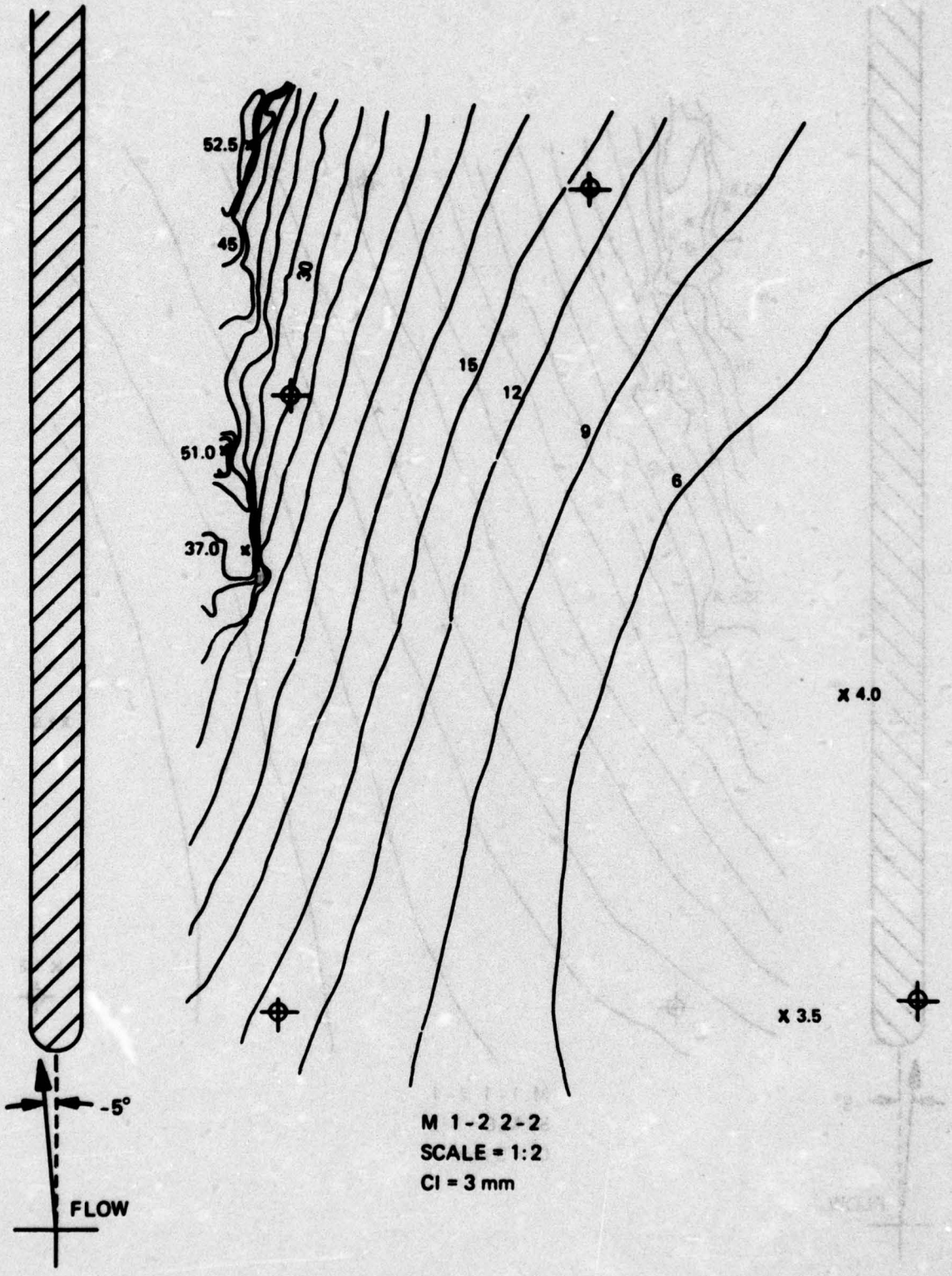

Figure 13 – Experimental Contours, θ = 5°, u = 5 Knots

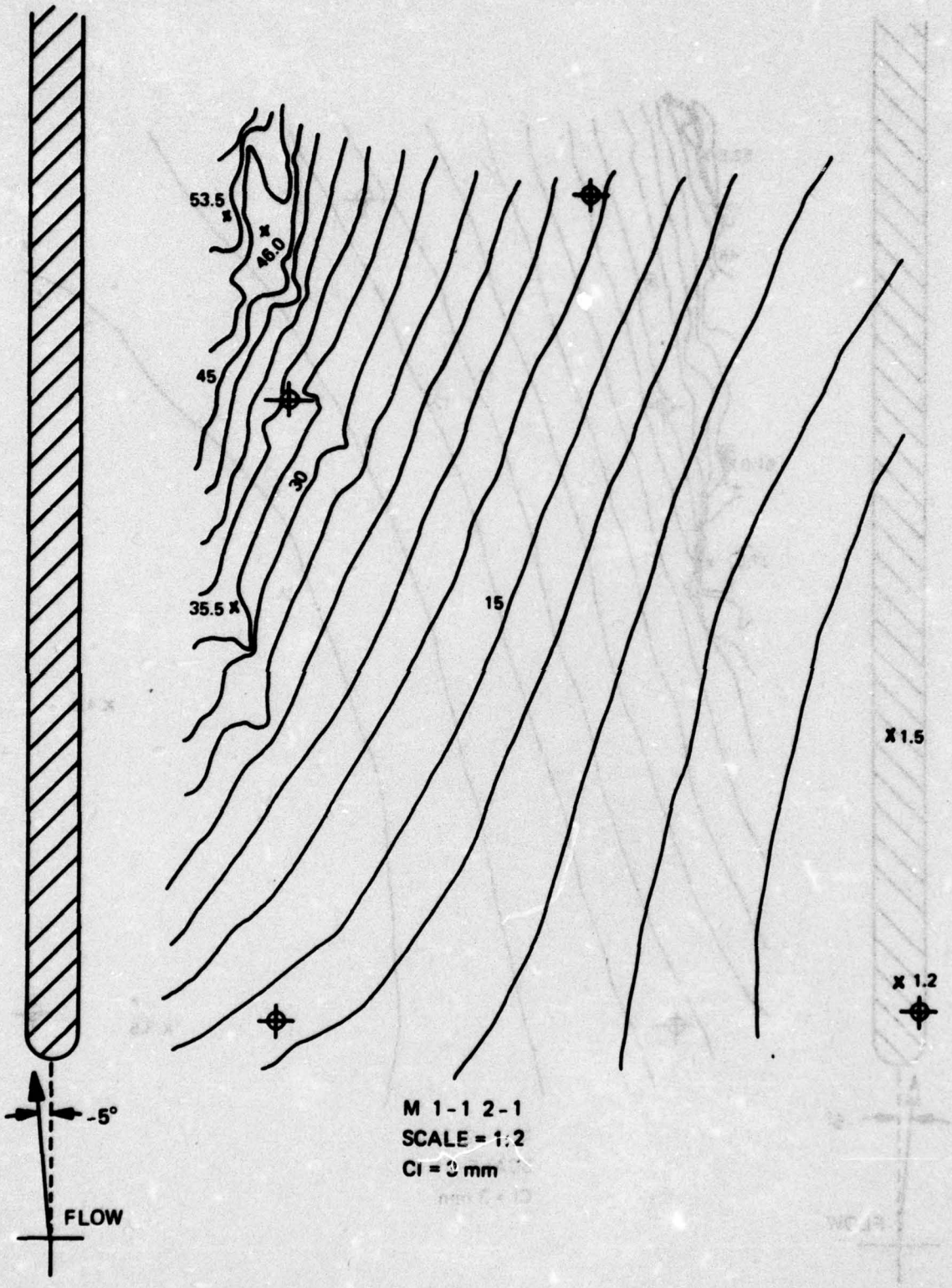

Figure 14 — Experimental Contours, θ = 5°, u = 6 Knots

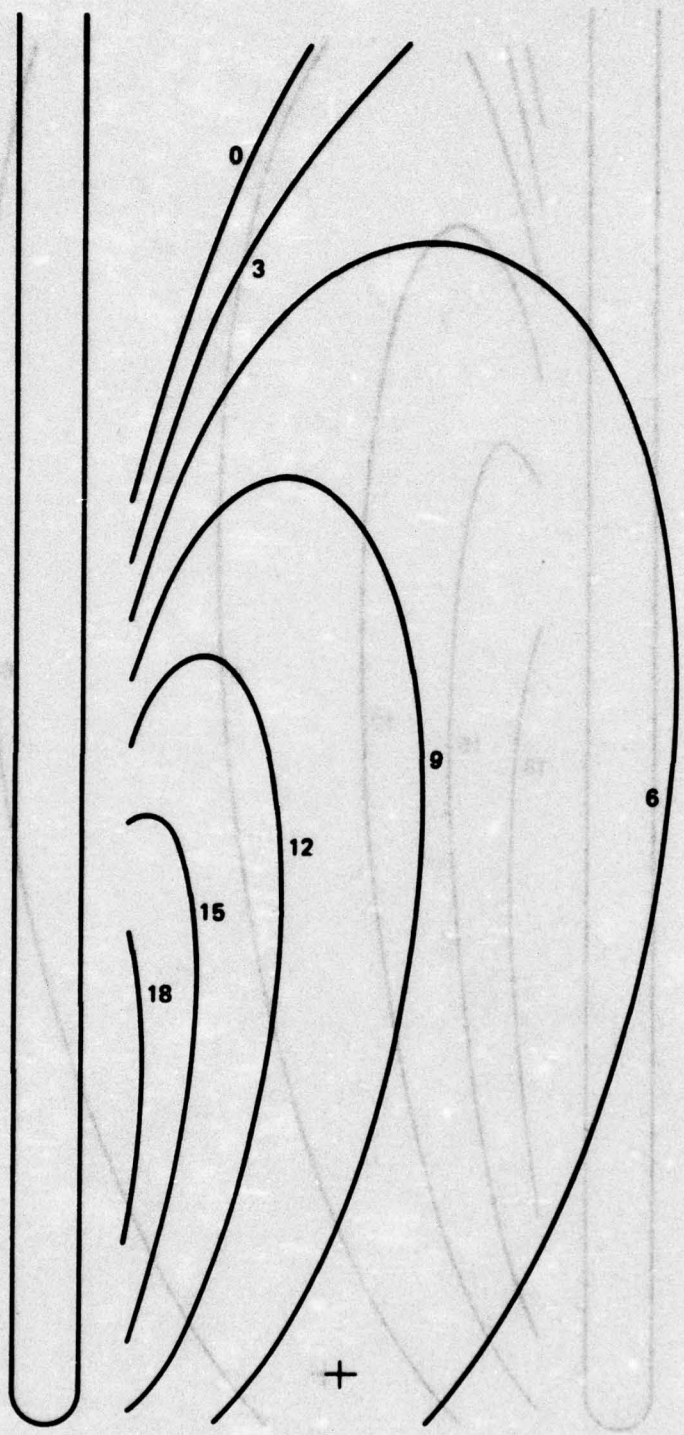

Figure 15 – Theoretical Contours, θ = 0, u = 4 Knots

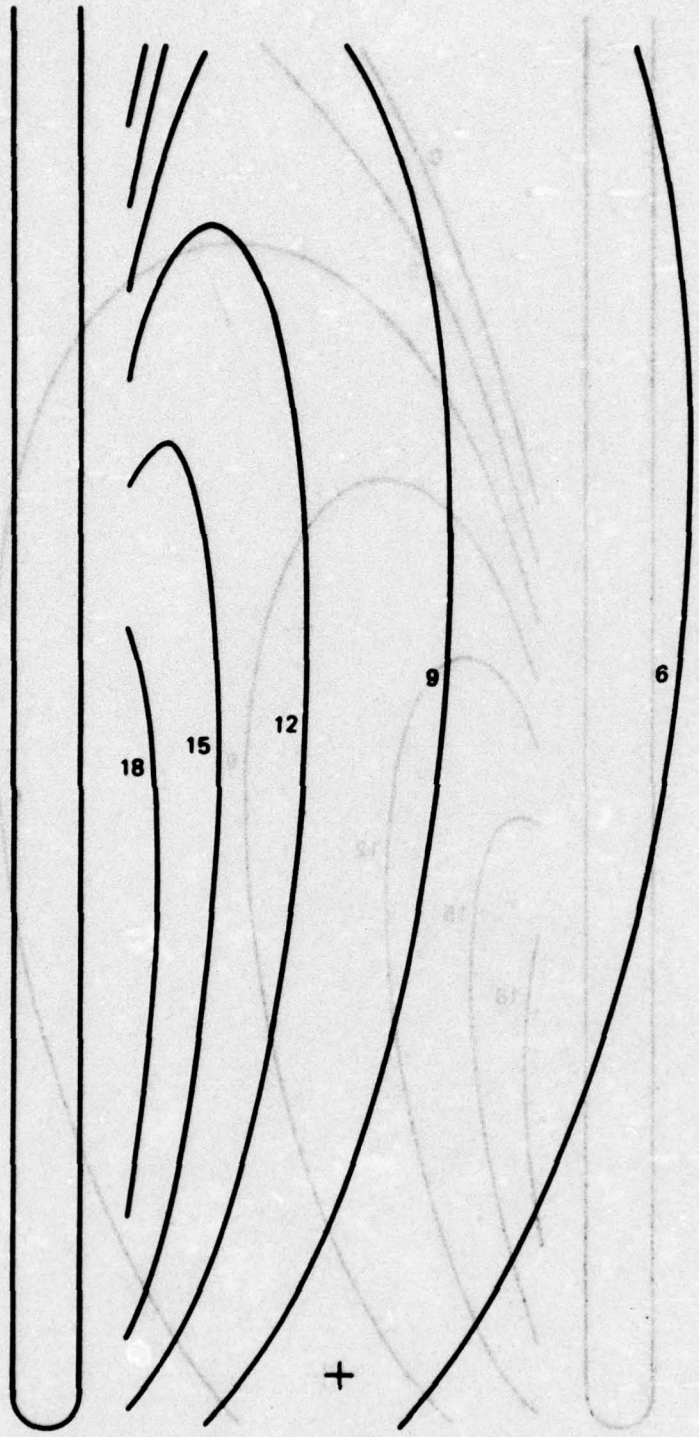

CONTOUR INTERVAL = 3 mm

Figure 16 – Theoretical Contours, θ = 0, u = 6 Knots

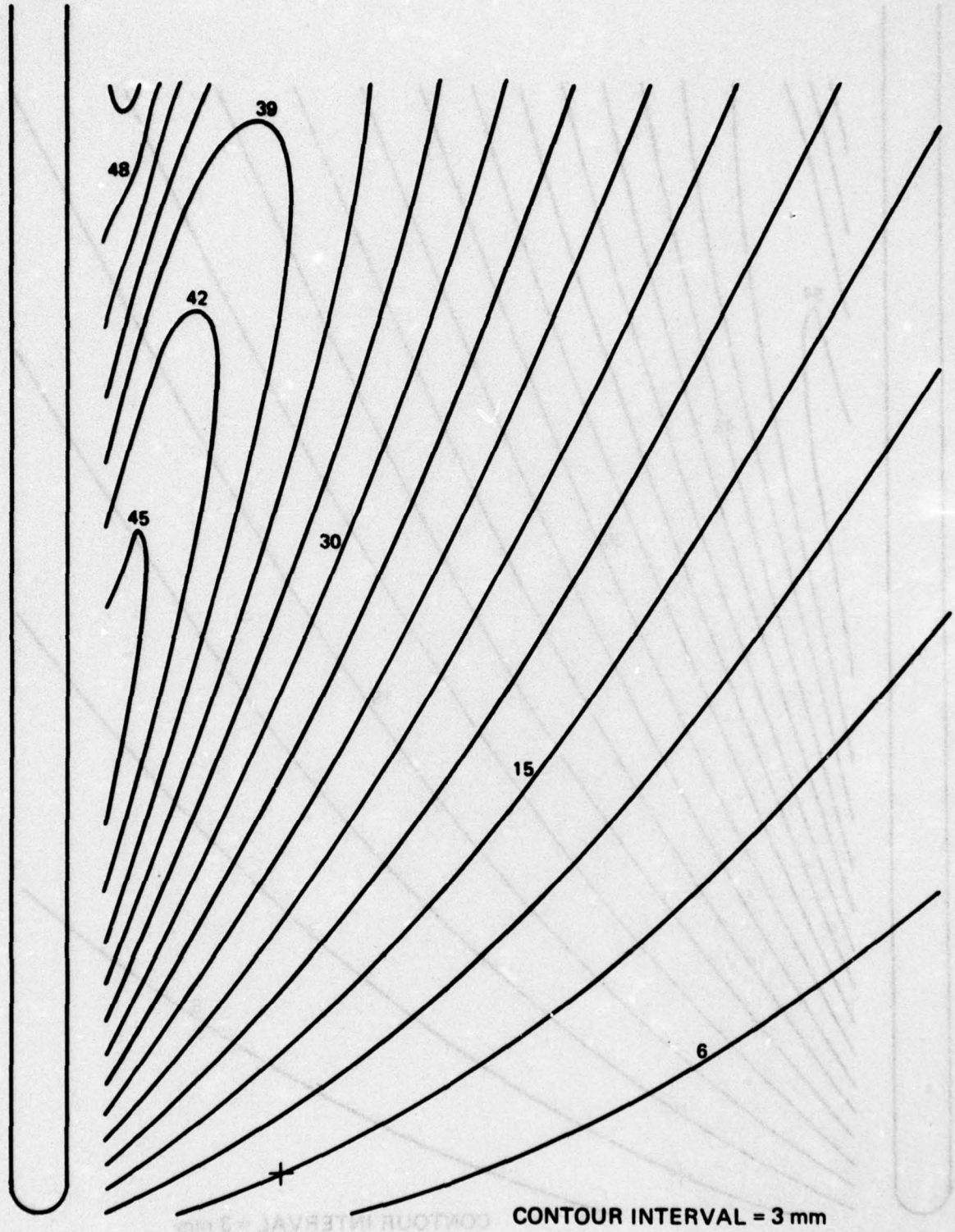

Figure 17 – Theoretical Contours, θ = 5°, u = 4 Knots

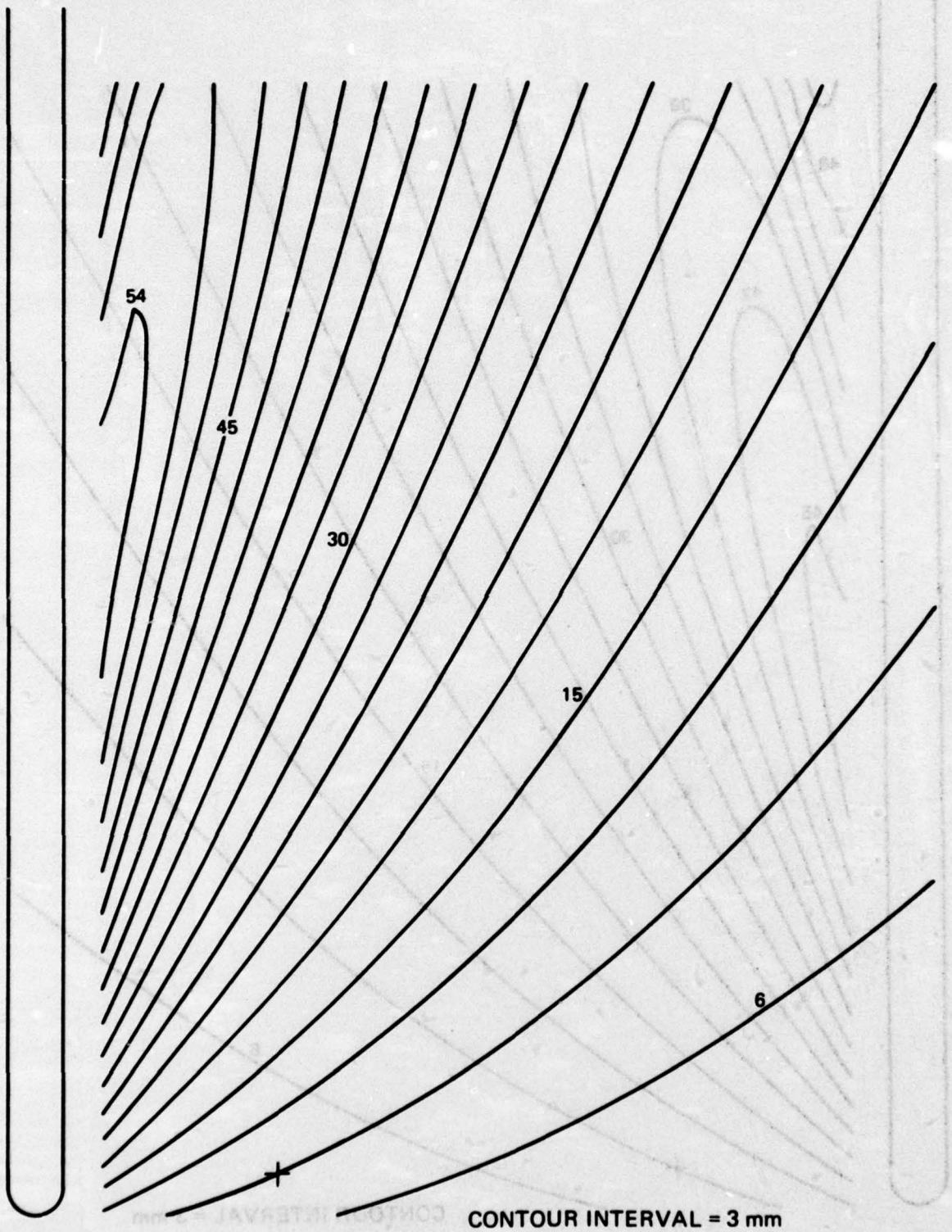

Figure 18 – Theoretical Contours, θ = 5°, u = 5 Knots

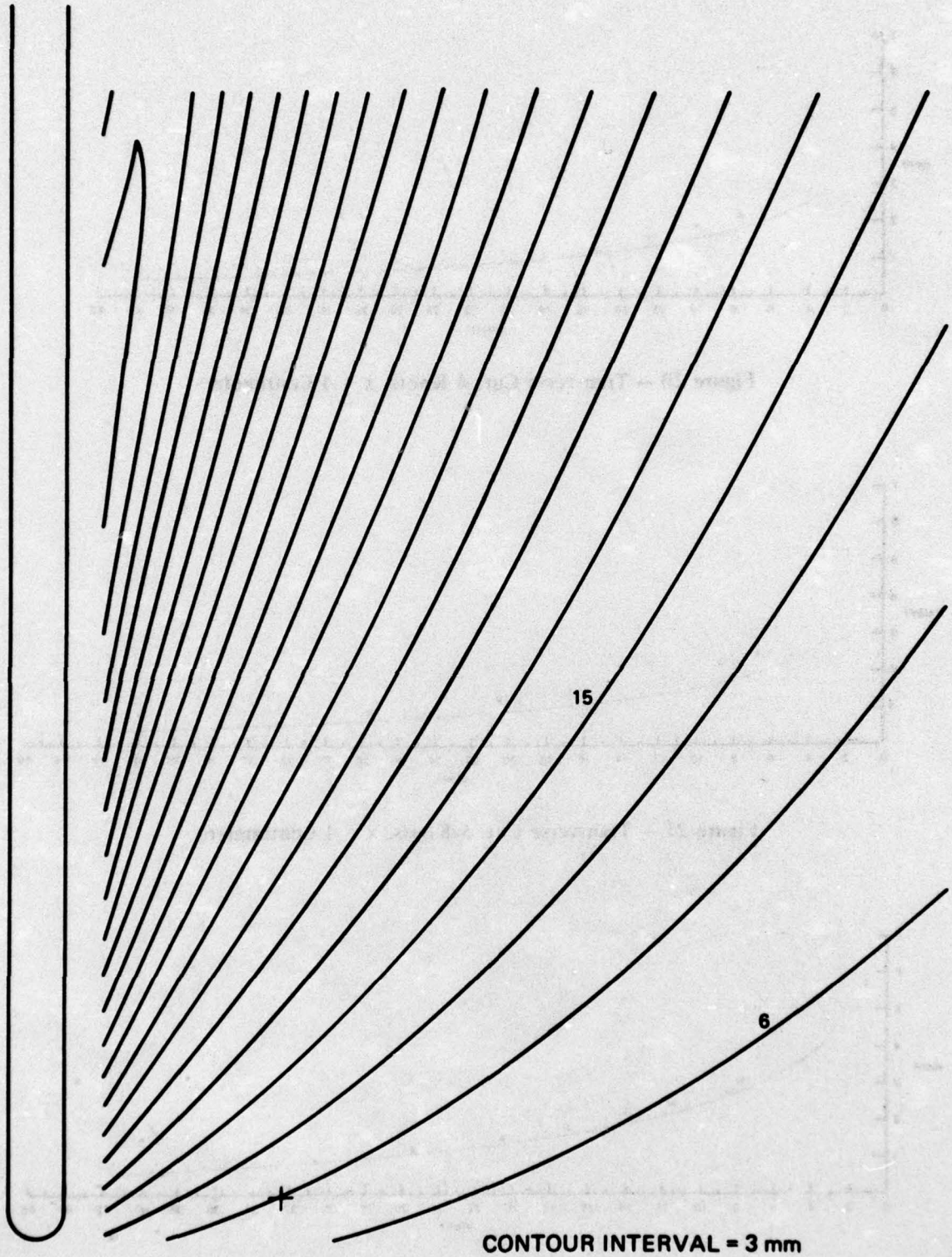

Figure 19 – Theoretical Contours, θ = 5°, u = 6 Knots

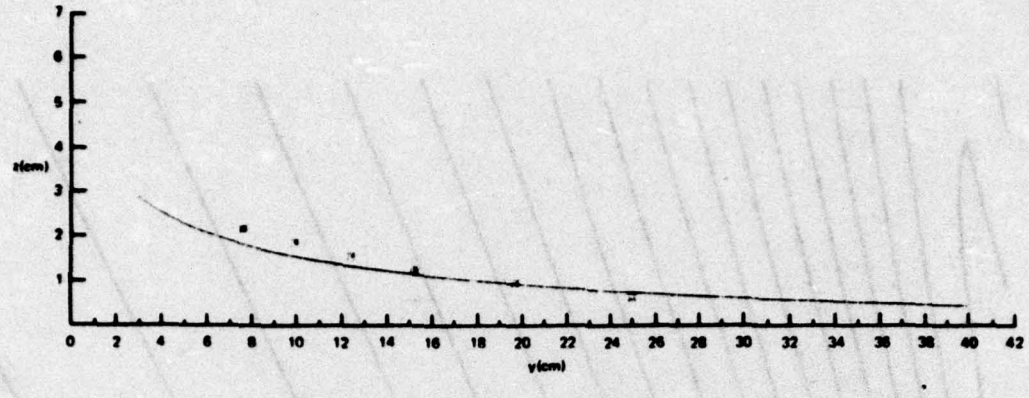

Figure 20 – Transverse Cut, 4 Knots, x = 4 Centimeters

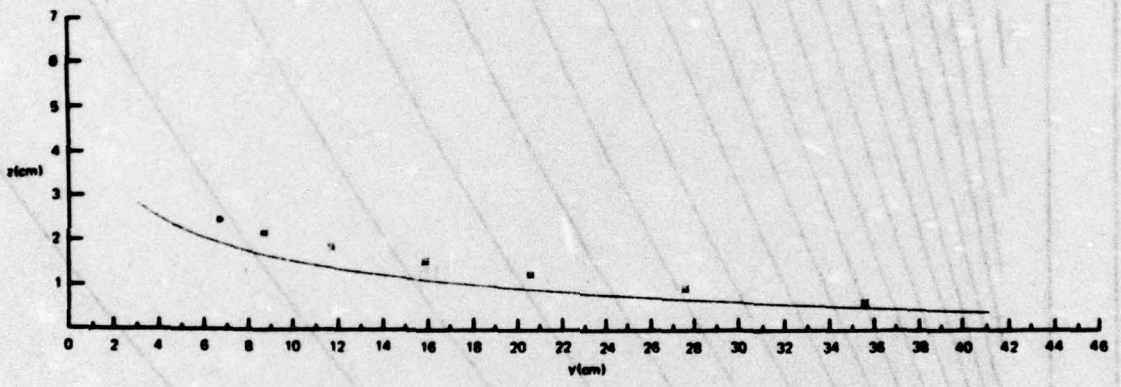

Figure 21 – Transverse Cut, 5 Knots, x = 4 Centimeters

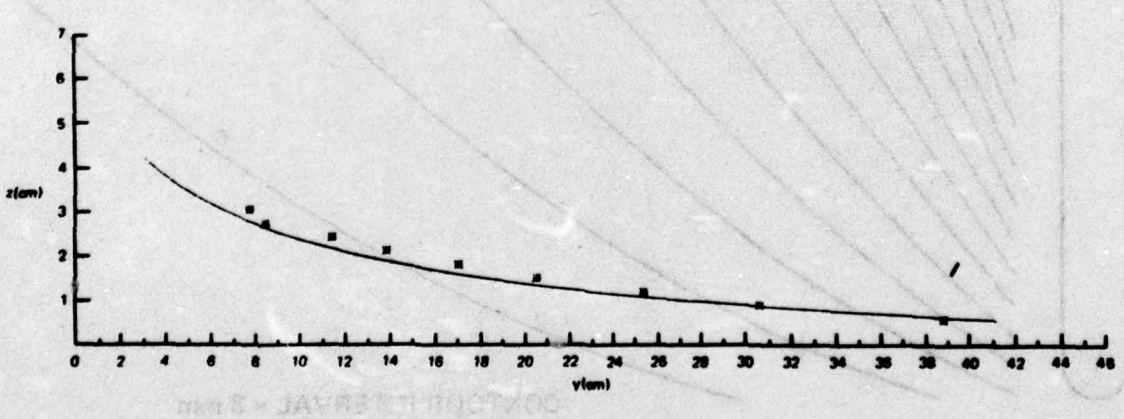

Figure 22 – Transverse Cut, 6 Knots, x = 4 Centimeters

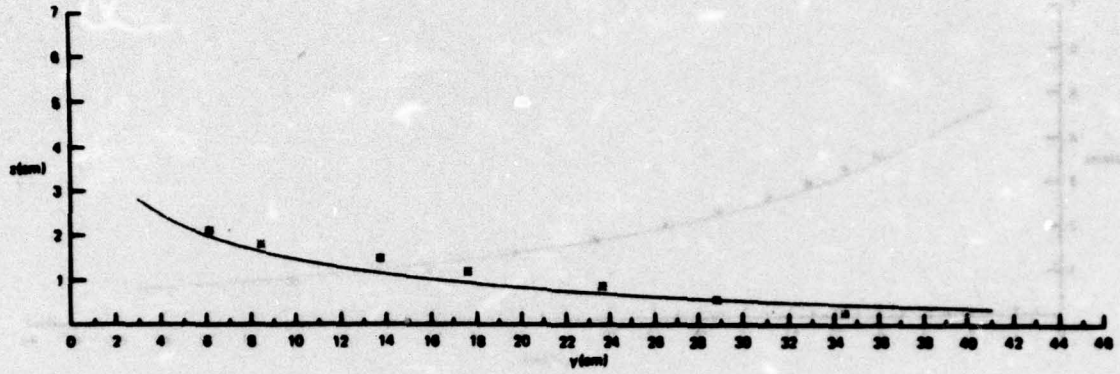

Figure 23 – Transverse Cut, 4 Knots, x = 8 Centimeters

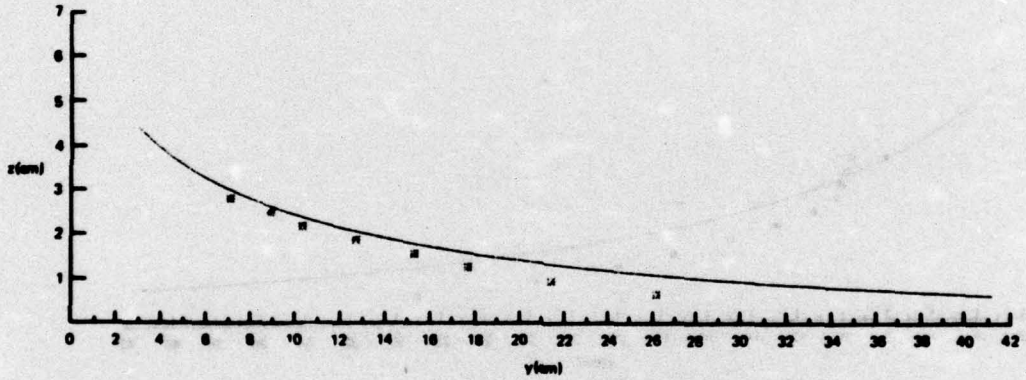

Figure 24 – Transverse Cut, 5 Knots, x = 8 Centimeters

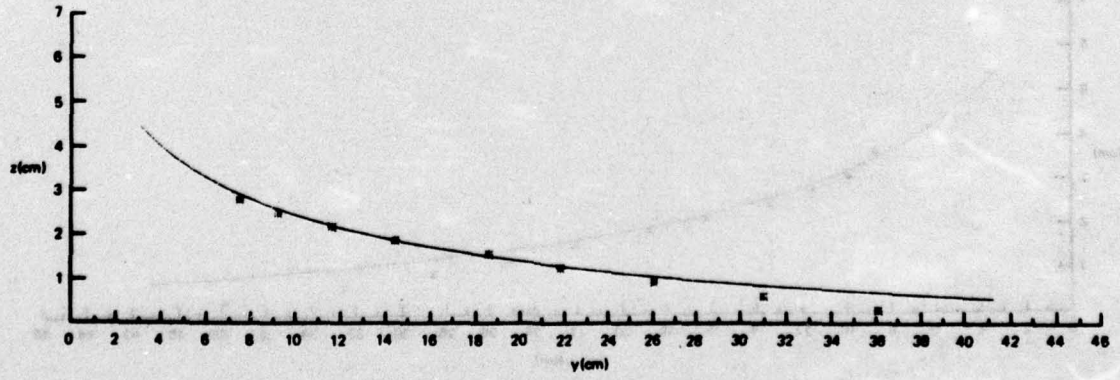

Figure 25 – Transverse Cut, 6 Knots, x = 8 Centimeters

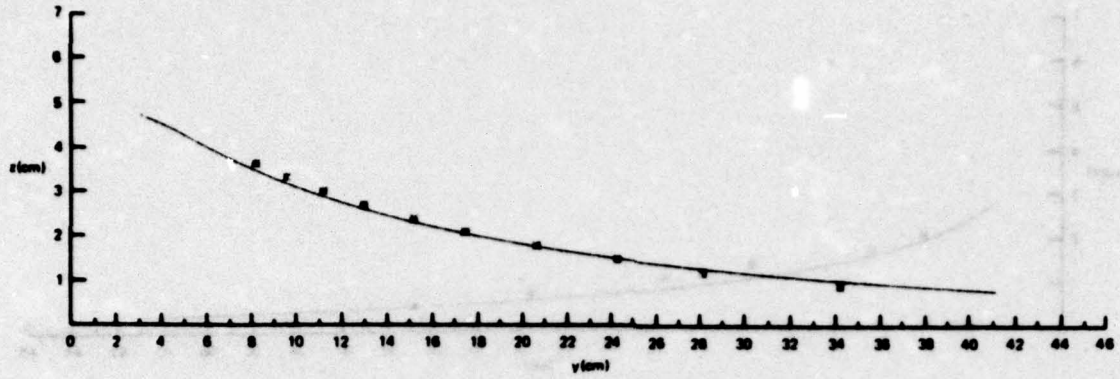

Figure 26 – Transverse Cut, 4 Knots, x = 12 Centimeters

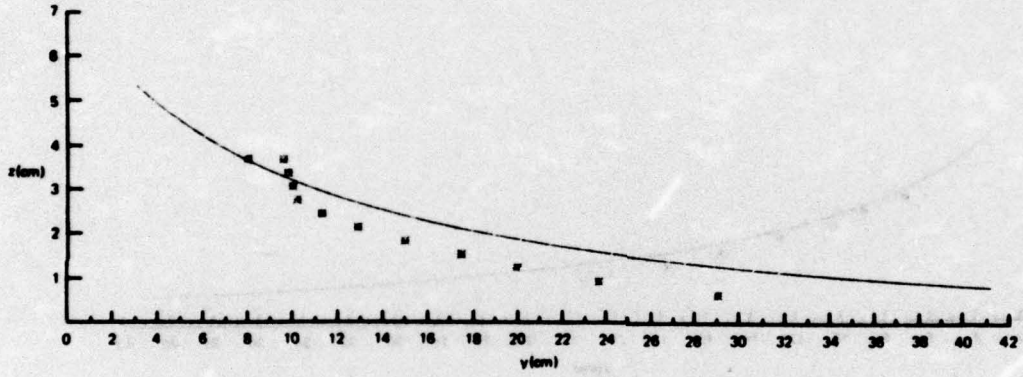

Figure 27 – Transverse Cut, 5 Knots, x = 12 Centimeters

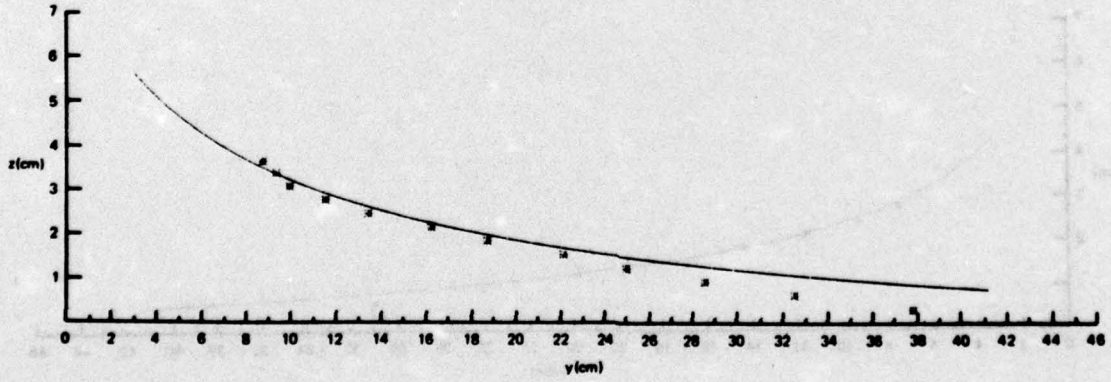

Figure 28 – Transverse Cut, 6 Knots, x = 12 Centimeters

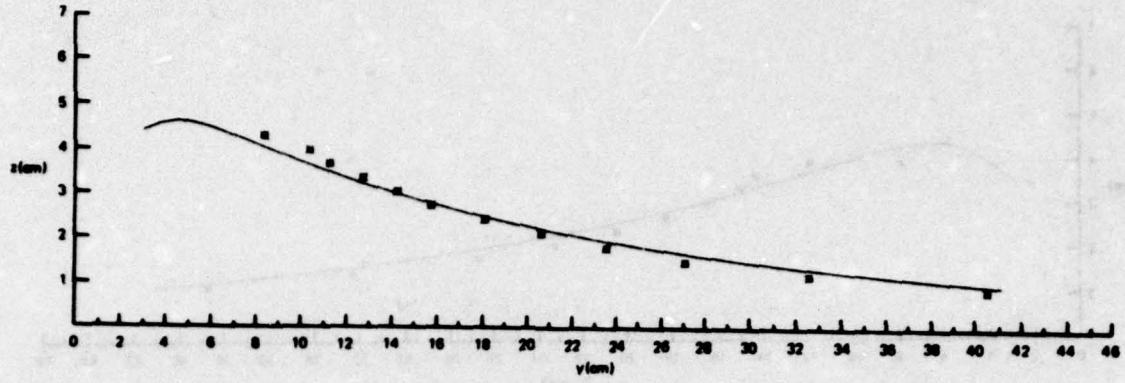

Figure 29 – Transverse Cut, 4 Knots, x = 16 Centimeters

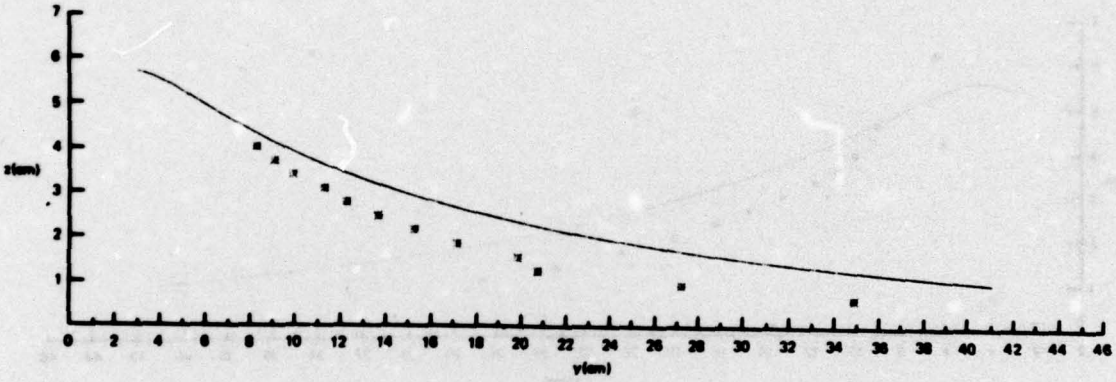

Figure 30 – Transverse Cut, 5 Knots, x = 16 Centimeters

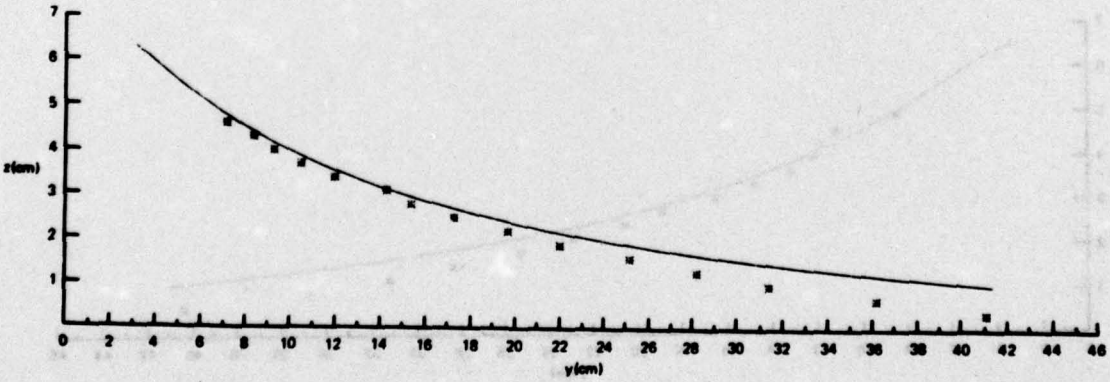

Figure 31 – Transverse Cut, 6 Knots, x = 16 Centimeters

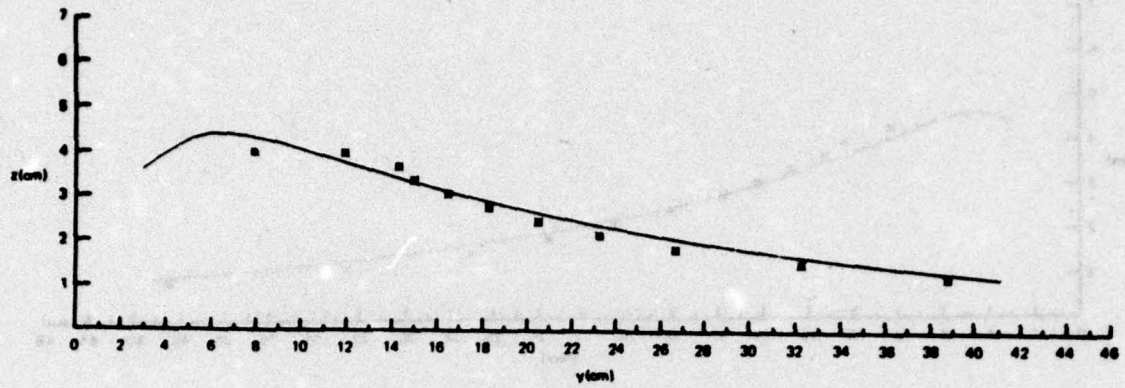

Figure 32 – Transverse Cut, 4 Knots, x = 20 Centimeters

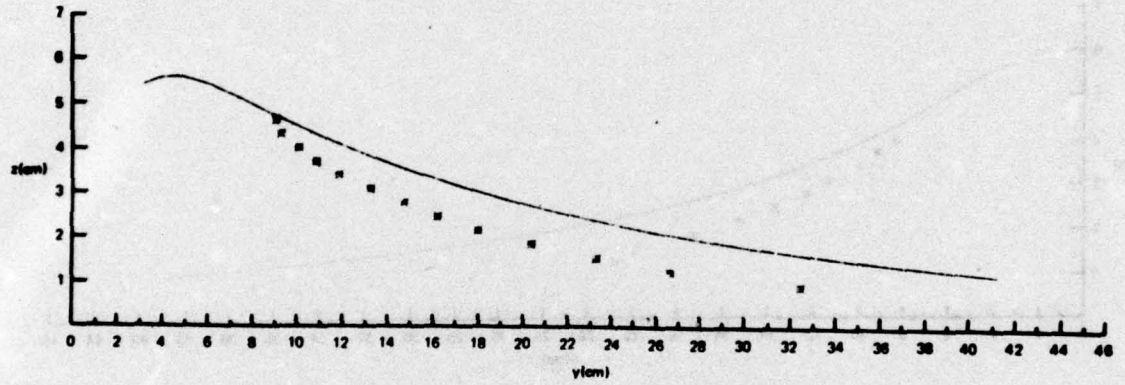

Figure 33 – Transverse Cut, 5 Knots, x = 20 Centimeters

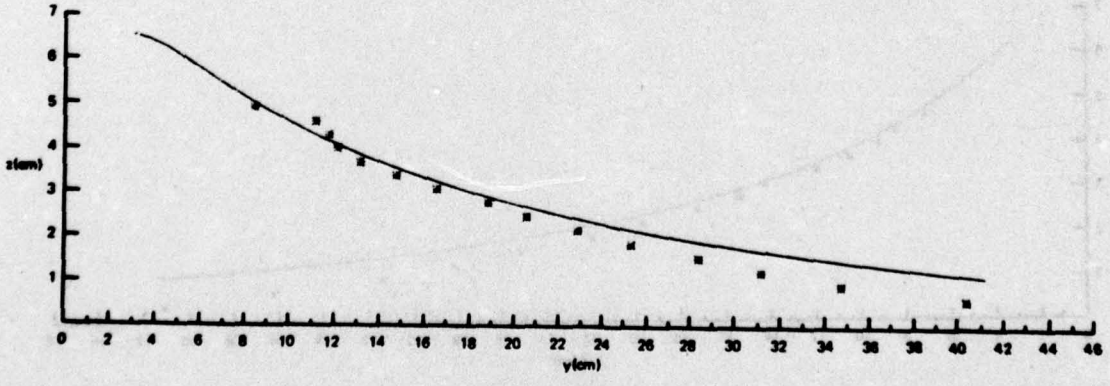

Figure 34 – Transverse Cut, 6 Knots, x = 20 Centimeters

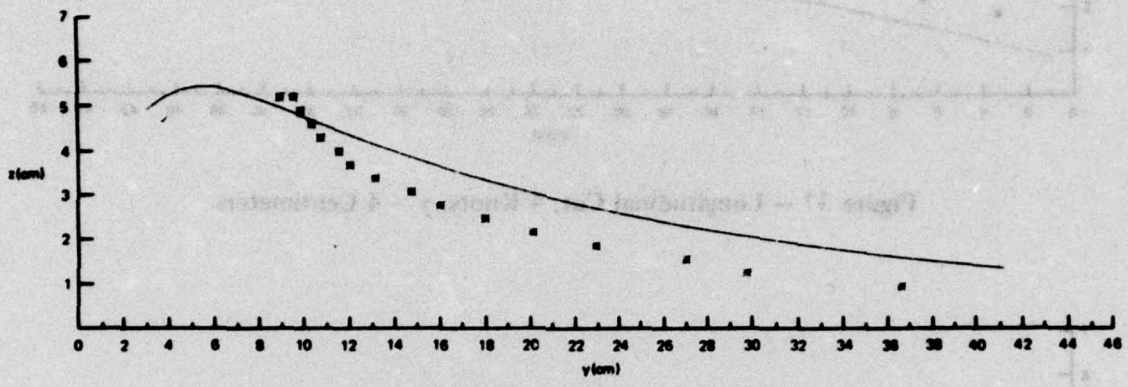

Figure 35 – Transverse Cut, 5 Knots, x = 23 Centimeters

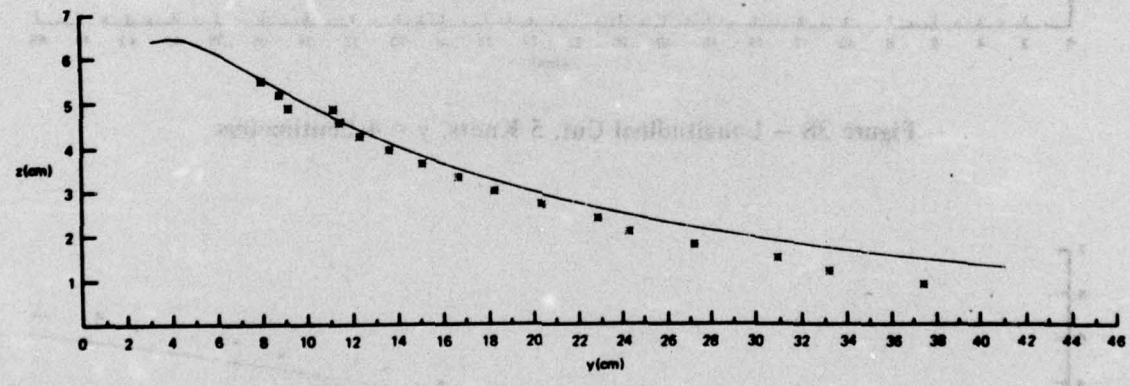

Figure 36 – Transverse Cut. 6 Knots, x = 23 Centimeters

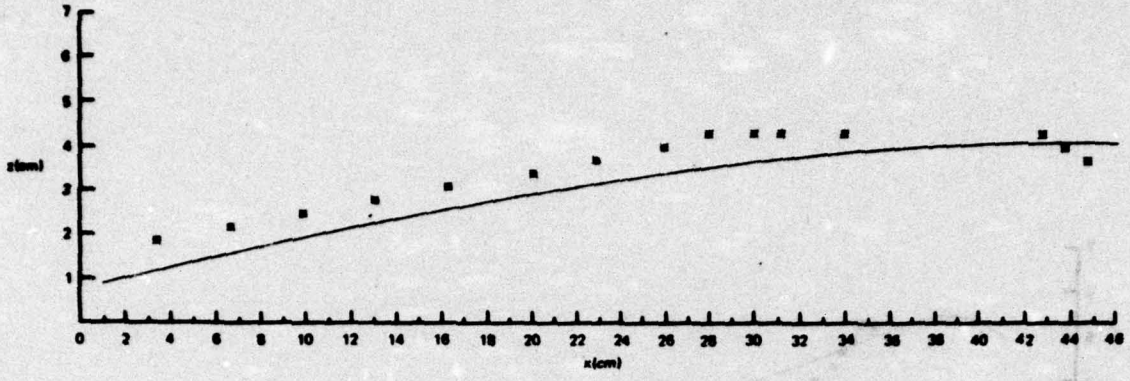

Figure 37 – Longitudinal Cut, 4 Knots, y = 4 Centimeters

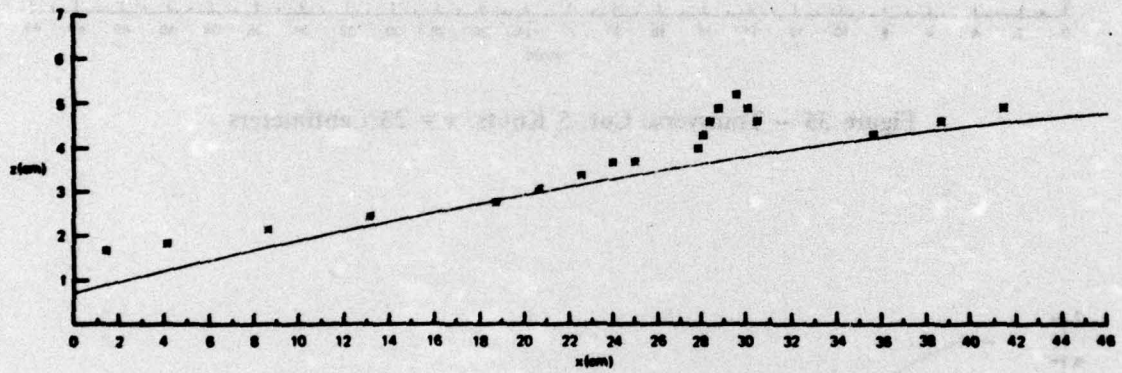

Figure 38 – Longitudinal Cut, 5 Knots, y = 4 Centimeters

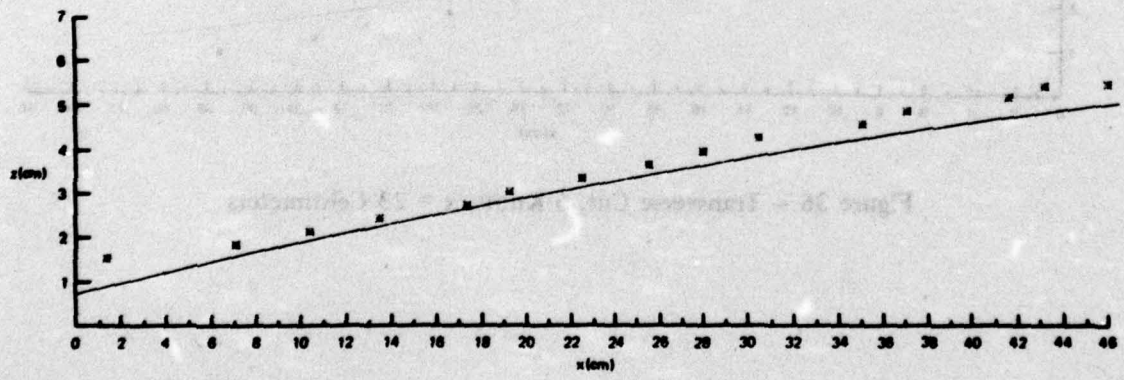

Figure 39 – Longitudinal Cut, 6 Knots, y = 4 Centimeters

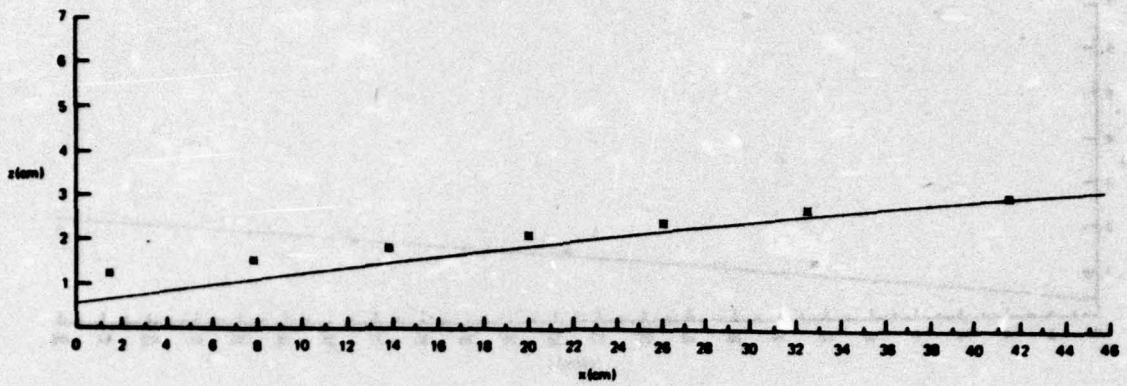

Figure 40 – Longitudinal Cut, 4 Knots, y = 8 Centimeters

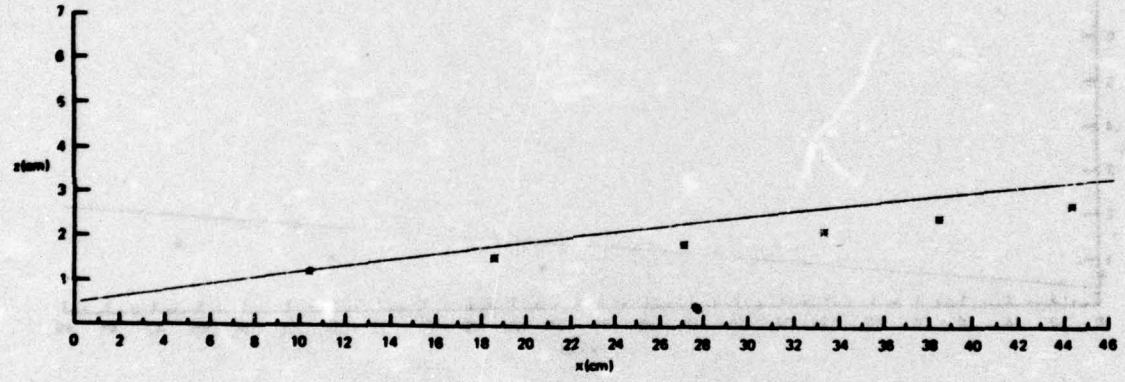

Figure 41 – Longitudinal Cut, 5 Knots, y = 8 Centimeters

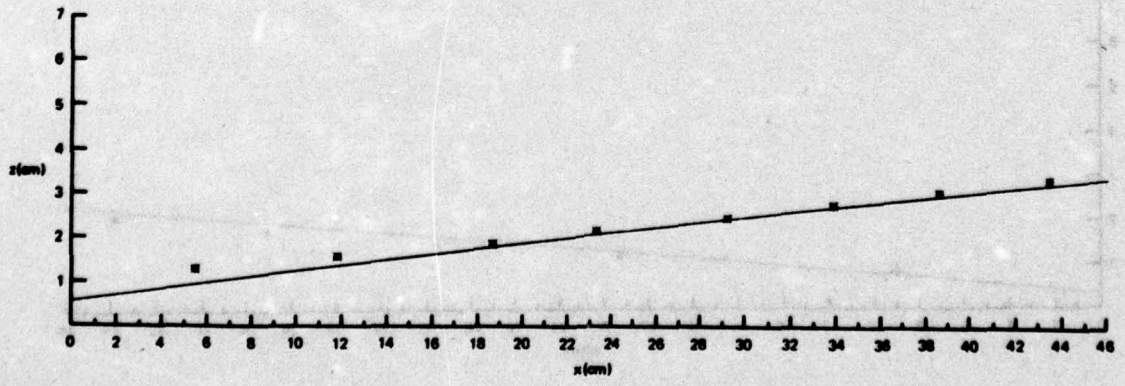

Figure 42 – Longitudinal Cut, 6 Knots, y = 8 Centimeters

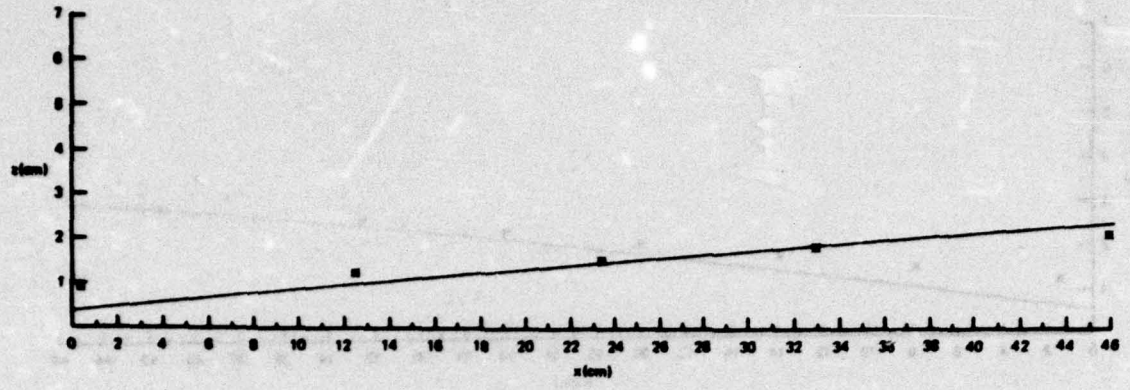

Figure 43 – Longitudinal Cut, 4 Knots, y = 12 Centimeters

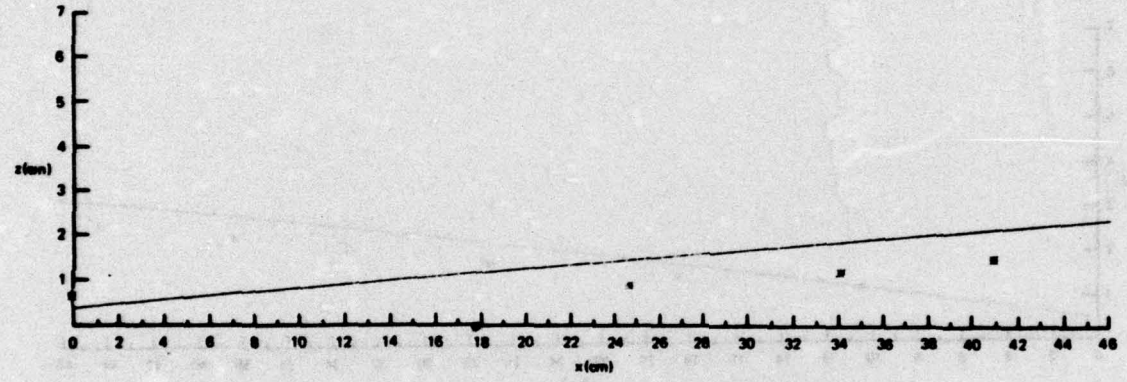

Figure 44 – Longitudinal Cut, 5 Knots, y = 12 Centimeters

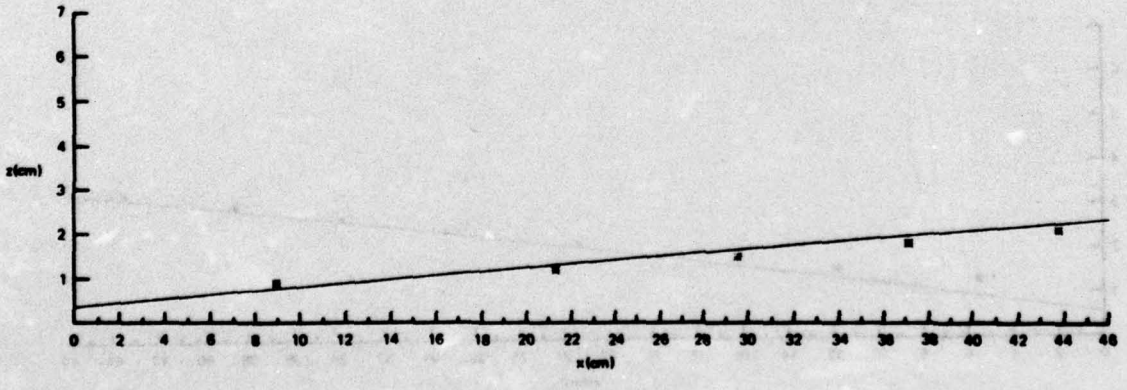

Figure 45 – Longitudinal Cut, 6 Knots, y = 12 Centimeters

INITIAL DISTRIBUTION

Copies	
1	WES
1	CHONR/438 Cooper
2	NRL 1 Code 2027 1 Code 2627
1	ONR/Boston
1	ONR/Chicago
1	ONR/Pasadena
1	ONR/San Francisco
1	NORDA
1	NOO/Lib (Naval Oceanographic Office)
5	USNA 1 Tech Lib 1 Nav Sys Eng Dept 1 Johnson 1 Bhattacheryya 1 Calisal
4	NAVPGSCOL 1 Library 1 T. Sarpkaya 1 Thaler 1 Garrison
1	NADC
1	NELC/Lib
3	NUC, San Diego 1 Library 1 Lang 1 Higdon
1	NSC/712 D. Humphreys
1	NCEL/Code 131
1	NSWC, Dahlgren
1	NUSC/Lib
4	NAVSEA 1 SEA 03221 1 SEA 032 1 SEA 03512/Pierce 1 SEA 037
1	NAVFAC/Code 032C

Copies	
1	NAVSHIPYD PTSMH/Lib
1	NAVSHIPYD PHILA/Lib
1	NAVSHIPYD NORVA/Lib
1	NAVSHIPYD CHASN/Lib
1	NAVSHIPYD LBEACH/Lib
2	NAVSHIPYD MARE 1 Library 1 Code 250
1	NAVSHIPYD BREM/Lib
1	NAVSHIPYD PEARL/Code 202.32
10	NAVSEC 1 SEC 6034B 1 SEC 6110.01 1 SEC 6114 1 SEC 6114P 1 SEC 6120 1 SEC 6136 1 SEC 6136/Covich 1 SEC 6114D 1 SEC 6120E 1 SEC 6136/Comstock
1	NAVSEC, NORVA/6660.03 Blount
12	DDC
1	AFOSR/NAM
1	AFFOL/FYS, J. Olsen
1	NSF/Eng Lib
1	LC/Sci & Tech
1	DOT/Lib TAD-491.1
2	MMA 1 Capt McClean 1 Library
1	NBS/Klebanoff
1	MARAD/Lib
5	U. of Cal/Dept Naval Arch, Berkely 1 Eng Library 1 Webster 1 Paulling 1 Wehausen

Copies	
2	U. of Cal, San Diego
	1 A.T. Ellis
	1 Scripps Inst Lib
3	CIT
	1 Aero Lib
	1 T.Y. Wu
	1 M. Plesset
1	City College, Wave Hill/Pierson
1	Catholic U. of Amer/Civil & Mech Eng
1	Colorado State U./Eng Res Cen
1	U. of Connecticut/Scottron
1	Cornell U./Sears
2	Florida Atlantic U.
	1 Tech Lib
	1 S. Dunne
1	U. of Hawaii/St. Denis
1	U. of Illinois/J. Robertson
3	U. of Iowa
	1 Library
	1 Landweber
	1 Kennedy
1	John Hopkins U./Phillips
1	Kansas State U./Nesmith
1	U. of Kansas/Civil Eng Lib
1	Lehigh U./Fritz Eng Lab Lib
6	MIT
	1 Library
	1 Yeung
	1 Mandel
	1 Abkowitz
	1 Newman
	1 Oakley
4	U. of Mich/NAME
	1 Library
	1 Ogilivie
	1 Beck
	1 Daoud
2	U. of Notre Dame
	1 Eng Lib
	1 Strandhagen
2	New York U./Courant Inst
	1 A. Peters
	1 J. Stoker

Copies	
1	Penn State/Arl/B. Parkin
1	Princeton U./Mellor
6	SIT
	1 Library
	1 Breslin
	1 Savitsky
	1 Dalzell
	1 Fridsma
	1 Kim
1	U. of Texas/Arl Lib
1	Utah State U./Jeppson
2	Southwest Res Inst
	1 Applied Mech Rev
	1 Abramson
2	Stanford U.
	1 Eng Lib
	1 R. Street
1	Stanford Res Inst/Lib
2	U. of Washington
	1 Eng Lib
	1 Mech Eng/Adee
3	Webb Inst
	1 Library
	1 Lewis
	1 Ward
1	Woods Hole/Ocean Eng
1	Worchester PI/Tech Lib
1	SNAME/Tech Lib
1	Bethlehem Steel/Sparrows Point
1	Bethlehem Steel/New York/Lib
1	Bolt, Beranek & Newman/Lib
1	Exxon, NY/Design Div, Tank Dept
1	General Dynamics, EB/Boatwright
1	Gibbs & Cox/Tech Info
5	Hydronautics
	1 Library
	1 E. Miller
	1 M. Tulin
	1 V. Johnson
	1 C.C. Hsu

Copies	
2	Lockheed, Sunnyvale
	1 Potash
	1 Chung
2	McDonnell Douglas, Long Beach
	1 J. Hess
	1 T. Cebeci
1	Newport News Shipbuilding/Lib
1	Nielsen Eng & Res
1	Oceanics
1	Rockwell International/B. Ujihara
1	Sperry Rand/Tech Lib
1	Sun Shipbuilding/Chief Naval Arch
2	American Bureau of Shipping
	1 Lib
	1 Cheng
1	Robert Taggart
1	Tracor
1	Maritime Research Information Service

CENTER DISTRIBUTION

Copies	Code	
1	117	R.M. Stevens
1	1170	S. Hawkins
1	1500	W.E. Cummins
1	1504	V.J. Monacella
1	1506	M.K. Ochi
1	1507	D. Cieslowski
1	1512	J.B. Hadler
1	1520	R. Wermter
1	1521	P. Pien
1	1524	Y.T. Shen
1	1524	W.C. Lin
1	1524	A.M. Reed
1	1532	G. Dobay
1	1532	M. Wilson
1	1540	W.B. Morgan
1	1552	J.H. McCarthy
1	1552	N. Salvesen
10	1552	R.B. Chapman
1	1542	B. Yim
1	1560	G. Hagen
1	1561	C.M. Lee
1	1562	M. Martin
1	1564	J. Feldman
1	1568	G. Cox
1	1568	E.A. Baitis
1	1568	W.R. McCreight
1	1572	M.D. Ochi
1	1572	E. Zarnick
1	1576	W.E. Smith
30	5214.1	Reports Distribution
1	5221	Unclassified Library (C)
1	5221	Unclassified Library (A)